Characterization and Sensitivity Analysis of 6 Meter Cassegrain Antenna

THESIS

James L. Harris, B.S.E.E., Captain, USAF
AFIT-ENG-MS-20-M-025

DEPARTMENT OF THE AIR FORCE
AIR UNIVERSITY

AIR FORCE INSTITUTE OF TECHNOLOGY

Wright-Patterson Air Force Base, Ohio

AFIT-ENG-MS-20-M-025

Characterization and Sensitivity Analysis of 6 Meter Cassegrain Antenna

THESIS

Presented to the Faculty
Department of Electrical and Computer Engineering
Graduate School of Engineering and Management
Air Force Institute of Technology
Air University
Air Education and Training Command
in Partial Fulfillment of the Requirements for the
Degree of Master of Science in Electrical Engineering

James L. Harris, B.S.E.E.,
Captain, USAF

March 26, 2020

AFIT-ENG-MS-20-M-025

Characterization and Sensitivity Analysis of 6 Meter Cassegrain Antenna

THESIS

James L. Harris, B.S.E.E.,
Captain, USAF

Committee Membership:

Andrew J. Terzuoli, Ph.D
Chair

Peter J. Collins, Ph.D
Member

Daniel J. Emmons, Ph.D
Member

AFIT-ENG-MS-20-M-025

Abstract

This paper will characterize a 6 meter in diameter cassegrain antenna. The cassegrain antenna is a special form of a dual reflector antenna which uses a main reflector following a parabolic curve and a sub reflector which follows a hyperbolic curve. Cassegrain style antennas have multiple parameters which can be tuned to achieve specific design goals. Performing a sensitivity analysis will establish relationships between design parameters, directivity, side lobe levels, and effects of strut geometry. The initial design parameters will be assumed based on typical values. Results from the sensitivity analysis will be used to provide a performance band for the 6m Cassegrain at select frequencies.

Table of Contents

List of Figures

Figure Page

List of Tables

Table Page

Characterization and Sensitivity Analysis of 6 Meter Cassegrain Antenna

I. Introduction

1.1 Problem Background

Dish style antennas are available in a multitude of configurations designed for a wide range of applications. The configuration which will be explored in this research is the axially fed dual reflector configuration. In 2016 a previous group performed a series of simulations to characterize a 10 m diameter cassegrain antenna. The organization which requested this work returned in 2018 requesting a characterization on a 6 m diameter cassegrain at two frequency bands, 9-11 and 13-15 GHz. At first glance it seems like the problem is simply solved by inserting numbers into a simulation tool. After some initial work trying this approach it became apparent that subtle changes to the antenna's parameters could significantly alter its performance. This work is intended to highlight how each of the antenna's parameters interact with each other and how single parameter changes impact the antenna's performance.

1.1.1 Dual Reflector Style Antennas

The cassegrain antenna was originally derived from the cassegrain telescope [2, 5, 6, 3]. Traditionally a cassegrain antenna is designed with a parabolic main reflector and a hyperbolic subreflector which are aligned axially [2]. There are also variations which use an offset design [7], specially shaped reflectors [8], and even frequency selective surfaces for the reflector surfaces [9, 10]. All of these variations open the door for application specific designs. The configuration which will be explored in this research is the axially fed dual reflector configuration with a hyperbolic contoured subreflector. This design was chosen based on the needs of the requesting organization.

1.2 Research Objectives

This work is intended to establish relationships between each of the design parameters and the overall beam pattern. With these established relationships, engineers and analysts will be able to quickly estimate the performance of an antenna design. Additionally, once limitations are fully established, solutions to exceed those limitations can be explored and proposed in future research. A secondary objective of this work is to provide a coherent single document which can be referenced for cassegrain antenna design. The objectives of this research will be achieved through the use of computational electromagnetics (CEM) and the analysis of its results.

1.3 Methodology

Establishing how alterations to the design parameters impacts antenna performance will be done systematically through simulations. The cassegrain antenna is a very mature design, and there is a broad availability of typical design values [11, 6, 12, 2]. Typical design values will be used to guide the parameter sensitivity analysis. Values for each of the cassegrain antenna's parameters will be assumed based on the previous work. Comparing the results from the sensitivity analysis to the assumed values will illustrate the relationships between design parameters. This methodology will be fully developed and detailed in Chapter 3.

1.4 Assumptions and Limitations

Assumptions and limitations need to be established to help guide the scope of this work. The antenna being characterized is a 6 m cassegrain antenna. There is not a specific make, model, manufacturer, location, or specific application identified for this antenna. A physical model with an attached coordinate system is not provided. This leads to the application of some “best case” rules, and assigning a coordinate system based on simplifying the problem set. All surfaces will be assumed to be a perfect electrical conductor (PEC). Choosing to evaluate all of the materials as PEC will slightly limit the accuracy of the simulations. However, this will provide a “best case” baseline. Actual materials will have loss effects, surface changes due to heating effects, resistivity, and positional tolerances from construction techniques. All of this is outside the scope of this work, and could be used as research topics for future works.

The main reflector diameter will drive many of the other parameters to be evaluated. In this work the main reflector diameter will be limited to 6 m. Previously, work was completed to characterize a 10 m cassegrain antenna. The parameters used to generate those results will be used as the assumed parameter values for the 6 m antenna. The frequencies of interest for this work will be limited to 9-11 and 13-15 GHz. These limitations do not limit the validity of this work in other frequency bands, and it is assumed that the data can be extrapolated to fit other frequencies and main dish diameters as required.

II. Background and Literature Review

This chapter presents the background and theoretical operation of the cassegrain antenna. Cassegrain antennas have been a subject of interest since the 1950s [13], and were originally derived from the cassegrain telescope [2]. Since this style antenna is akin to the cassegrain telescope, many of the geometrical relationships also apply to the dual reflector antenna. In this chapter the unique geometries of this style antenna will be described and discussed. Techniques for analyzing and simulating electrically large antennas will also be described and discussed. Specifically this means exploring physical optics (PO) and uniform theory of diffraction (UTD), and reviewing simulation software. This chapter will conclude with the presentation of various accepted rules of thumb for dual reflector antennas.

2.1 Previous Efforts for the 10 m Antenna

Previous efforts to characterize a 10 m cassegrain antenna for the 9-11 GHz band was completed in 2016. During this research the group was provided with assumed values as shown in Table 1. From this provided data the group determined the remaining dimensions they needed in order to complete the work.

The previous group started their determination of values by assuming that the depth of the main reflector was 1/5th that of the main reflector. This lead to the possibility to determine the focal length and focal length to diameter ratio. These

Table 1. Assumed Parameters provided to the original 10 m characterization work.

Parameter	**Provided Values**
Frequency Range	9-11 GHz
Main Dish Diameter	10 m
Subreflector Diameter	1m
Main Reflector Subreflector Distance	3m
Strut Locations	As seen in Figure 1

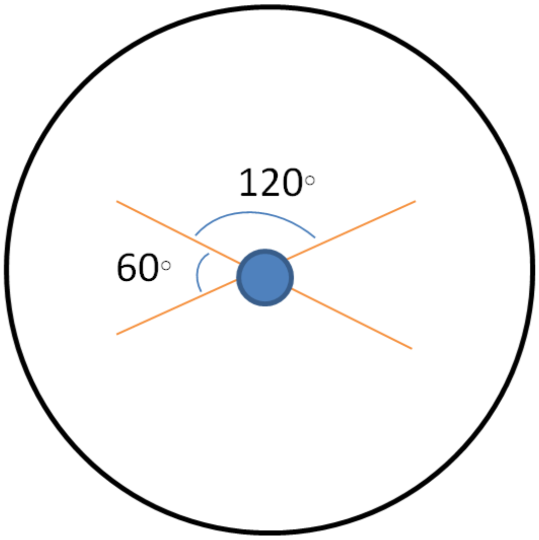

Figure 1. Strut angles referenced to each other.

values are sufficient to fully define the main reflector [2, 6, 12, 11, 3]. The group also made an assumption that the subreflector depth was 1/3 of its diameter, and then used the focal length of the main reflector to determine its vertex location. Determining the vertex location for the subreflector is valid when the feed's focal point is also assumed [2, 12].

Combining the information shown in Figure 2 and Figure 3 the previous group completed their work providing information on the main lobe and out to three side-

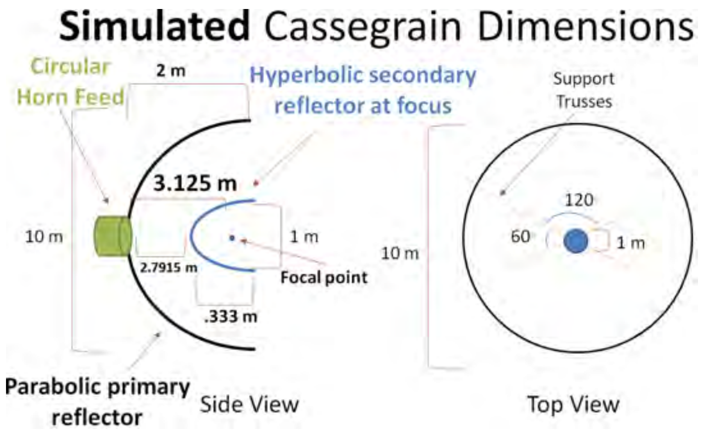

Figure 2. Image from previous work detailing the dimensions used in their simulations.

lobes. The information relayed a magnitudes for the lobes, locations, and a half power beamwidth. All of this information was portrayed for the various antenna pattern cuts as well as the frequencies of interest.

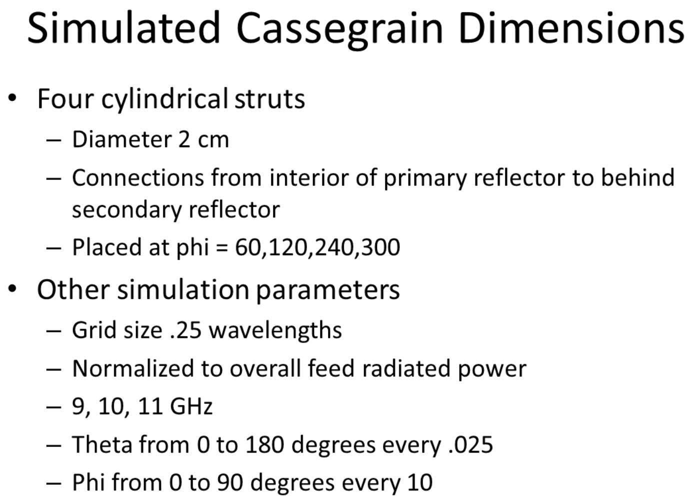

Simulated Cassegrain Dimensions

- Four cylindrical struts
  - Diameter 2 cm
  - Connections from interior of primary reflector to behind secondary reflector
  - Placed at phi = 60,120,240,300
- Other simulation parameters
  - Grid size .25 wavelengths
  - Normalized to overall feed radiated power
  - 9, 10, 11 GHz
  - Theta from 0 to 180 degrees every .025
  - Phi from 0 to 90 degrees every 10

Figure 3. Image from previous work detailing the struts and simulation parameters used in their simulations.

Overall, there was concurrence among the individuals involved with the project that the results were accurate. The available data from the previous work will be used as a comparison for this research effort. Comparing the results from the 10 m characterization to the 6 m characterization could provide insight into the scaling factors between these antennas.

2.2 Physical Optics

Before diving specifically into the geometry and properties of the cassegrain antenna, an understanding of PO is necessary. At the heart of PO lies the concept of ray tracing. Ray tracing is a technique which assumes all electromagnetic waves can be looked at as a combination of rays. Each ray is followed along its path to determine how it contributes to the field strengths in the far field. Along each ray's path, Snell's law of reflection is applied to any reflecting surface.

Physical optics began as a study of how light interacted with reflective surfaces and propagated through materials. This was later extended to high frequency waves. In PO, the wave is treated like a bundle of rays. In order to apply these principals to electromagnetics the surfaces must be much larger than the wavelength of any reflected waves. Another way of stating this, is that areas surrounding points of reflections must be relatively flat and smooth. This allows the application of law of reflections at each point successively.

While a full treatment of PO is an interesting topic, it is well outside of this work's scope. Highlights of PO are all that is required to understand how the geometry of cassegrain antennas work together. Law of reflection is the beginning point for understanding PO. Put simply, it states that a ray which is incident on a reflective surface will reflect away from that surface at an equal angle with respect to the surface.

$$\hat{n} \cdot \hat{s}^i = -\hat{n} \cdot \hat{s}^r \tag{1}$$

In Equation (1) $\hat{n}$ is a "unit surface normal" to the reflective surface at a point[14]. $\hat{s^i}$ is an incident ray and $\hat{s^r}$ is a reflected ray. Equation (1) says that a ray which is incident onto a reflective surface will have an equivalent reflected ray which can be seen by looking at the projections of each ray on to the plane of reflection. From Equation (1) Equation (2) follows where θ is the angle between the ray and .

$$cos(\theta^i) = cos(\theta^r) \tag{2}$$

Applying a cross product to $\hat{n}$ you will find the tangent to that surface. From this Equation (3) follows.

$$\hat{n} \times \hat{s}^i = \hat{n} \times \hat{s}^r \tag{3}$$

In electromagnetics it is well understood that the total field at a point is equivalent to incident field plus the scattered field.

$$E^t = E^i + E^s \tag{4}$$

In this simplified handling of PO, we are assuming that the incident field is reflected perfectly and without loss. However, the scattered field could be composed of losses, reflections, and diffraction. Since PO lacks the inclusion of things like diffraction and surface currents, shadow boundaries are setup. Shadow boundaries are areas where PO predicts that no fields will exist as result of neither incident nor reflected fields.

Figure 4 demonstrates shadow boundaries. In this figure the point S is a spherical wave source and there is a parabolic reflector between ymin and ymax. The areas outside of Region I are not predicted to have field contributions from the source.

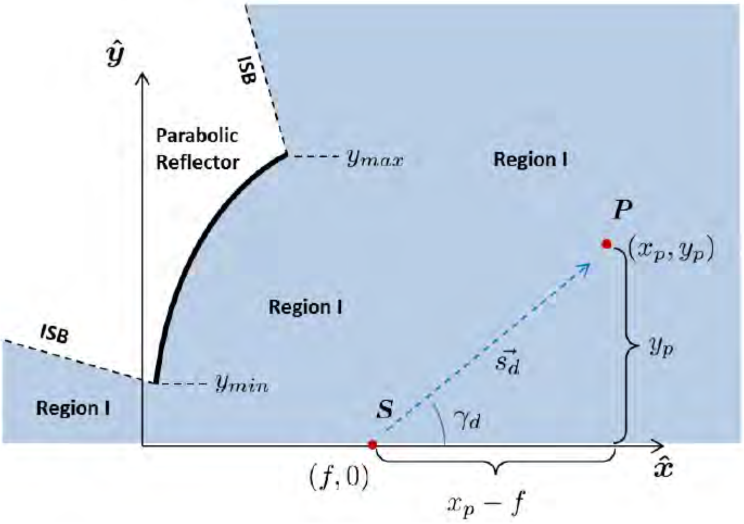

Figure 4. Example of incident shadow boundaries [1].

Since the areas outside of Region I do not have an incident or reflected field, the field strength is predicted to be 0. In Figure 4 the regions outlined in Region I will contain at a minimum an incident field component. The boundaries outlined here are incident shadow boundaries. There are also reflected shadow boundaries. Reflected waves are not predicted to be outside of these boundaries. In Figure 5, Region II predicts the area that will contain both an incident field and reflected field. Finding the areas in which the reflected field will exist requires an in-depth analysis of the reflecting body and where the source exists.

Notice in Figure 4 and Figure 5 that fields are not predicted to exist in the region "behind" the parabolic reflector. It is important to note this because in reality there will be fields which can exist. Depending on the specific location, the major factor contributing to the existence of fields in this area would be diffraction. The omission of diffraction effects can be a significant cause of errors between simulation and measurement. The Uniform Theory of Diffraction was created to bring reality and theory closer together.

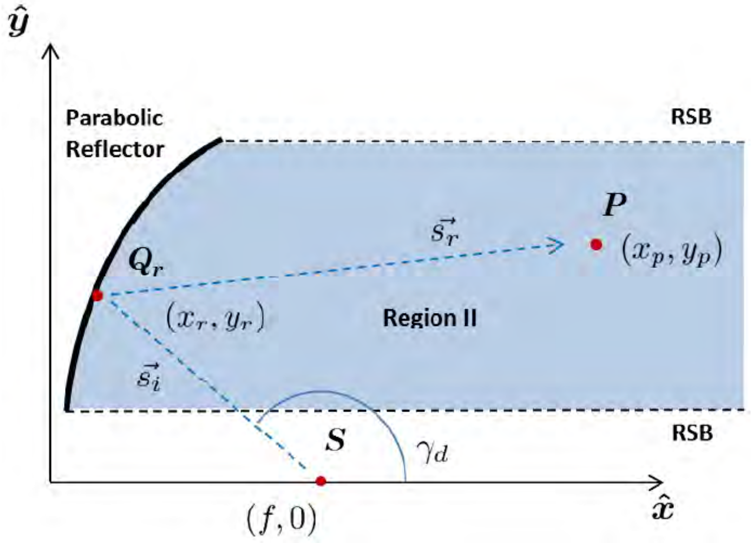

Figure 5. Example of reflected shadow boundaries [1].

2.3 Uniform Theory of Diffraction

The asymptotic techniques explored in PO do not fully describe how electromagnetic waves interact with surfaces. PO fails to accurately predict wave interaction with an edge or a wedge shaped geometry. This is where diffraction theories come into play.

Diffraction theories started with J.B. Keller postulating that diffracted rays exist when edges, corners, and vertices are illuminated [15]. From this postulate the initial description was that a cone of rays would be emitted from the diffraction point. Figure 6 illustrates this cone effect from a diffracted ray[3].

Initial applications of Keller's Geometrical Theory of Diffraction expressions fell short of describing wedges with curved faces. Additional studies expanded Keller's work and built the framework for UTD. UTD does address situations where curved faces are present at or near the diffraction points. Further explorations into UTD revealed that diffraction even occurs at discontinuity points of a curve as illustrated in Figure 7.

Generally the UTD expression for the diffracted field at a point is shown in Equation (5)

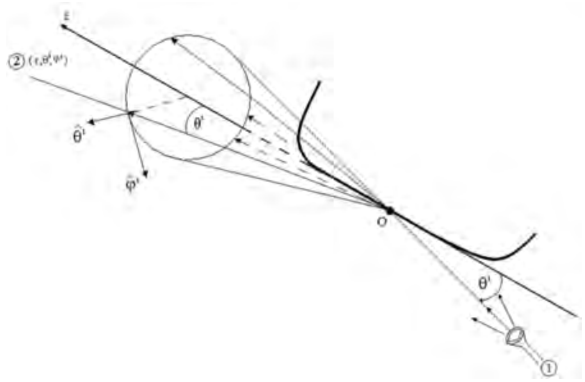

Figure 6. Theoretical diffraction from an edge [16].

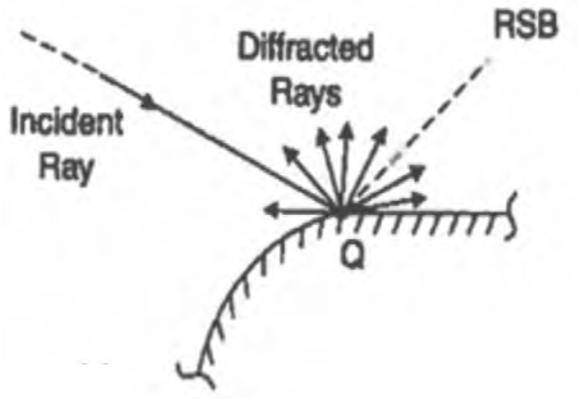

Figure 7. Theoretical diffraction from a curved edge [16].

$$U^d = [U^i(Q_e)D_{s,h} + \frac{1}{jk}\frac{\partial D_{s,h}}{\partial \phi'}\frac{\partial U^i(Q_{e)})}{\partial n}]\frac{e^{-jks}}{\sqrt{s}} \tag{5}$$

Where

s is the distance from point "a" point to point Q_e

U^i is the incident field at Q_e

$D_{s,h} = \frac{-e^{-j\frac{\pi}{4}}}{2\sqrt{2\pi k}}\left(\frac{F[kL^i a(\phi - \phi^{'})]}{cos(\frac{\phi - \phi^{'}}{2})} \mp \frac{F[kL^r a(\phi + \phi^{'})]}{cos(\frac{\phi + \phi^{'}}{2})}\right)$

$L^i = \frac{ss^{'}}{s + s^{'}}$

$L^r = s$

$a(\phi \pm \phi^{'}) = 2cos^2(\frac{\phi + \phi^{'}}{2})$

F[...] is the Fresnel transition function. In Equation (5) the angles ϕ and $\phi^{'}$ are angles related to the incident and reflected rays to a specific point. Figure 8 shows how these angles are related. A key point in applying UTD is identifying points where diffraction can occur. In Figure 8 the diffraction point is at the tip of a parabolic curve being used to represent the main reflector for a compact range reflector system [1]. This is the same diagram for the diffraction points at the edges of the main and subreflectors in a cassegrain antenna.

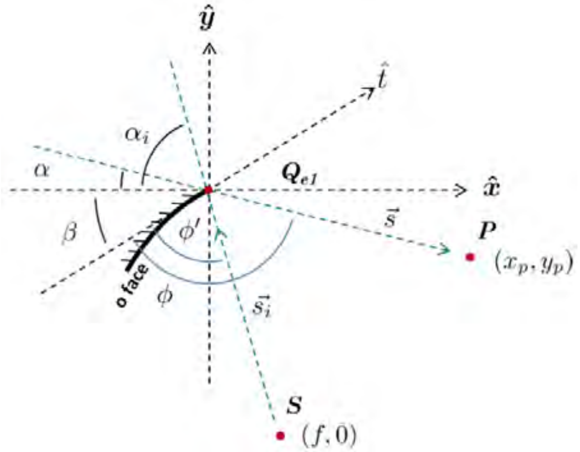

Figure 8. Angular relationships for a diffraction point at the end of a parabolic curve [1].

While a major component of UTD is diffraction, creeping waves also exist and are covered by UTD. Creeping waves can be thought of as a wavefront which follows the contour of the object. Combining the incident field, PO field, and the UTD field results in an accurate estimation of the total fields. As with PO,delving deeply into UTD is outside of the scope of this work. Many commercially available software packages provide simulations based on PO and UTD. In Section 2.5 three of the available software packages will be discussed. However, the general geometry of the cassegrain antenna will be discussed first.

2.4 Geometry of the Dual Reflector Antenna

Dual reflector antennas begin with 3 main components: the main reflector, subreflector, and the feed. Figure 9 shows a sample configuration of a cassegrain antenna. In this example the system is being viewed as a transmit antenna. The goal of the system is to redirect the energy of a feed into a tight beam. Traditionally, these systems are significantly larger physically than the design frequency's wavelength. When surfaces are disproportionately large compared to the wavelength, the surface is considered electrically large. Since these surfaces are electrically large the basic

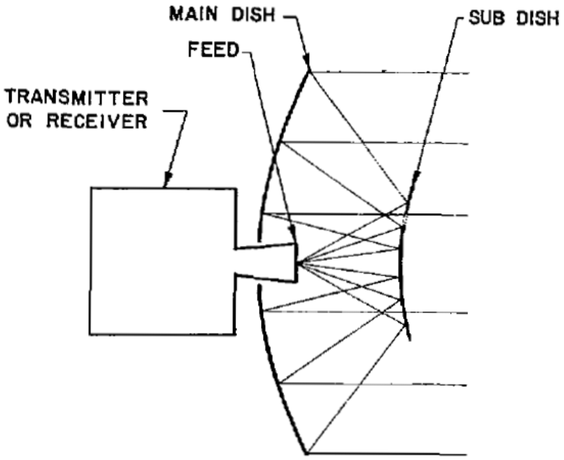

Figure 9. Geometry of the cassegrain antenna [2].

principals of geometric optics (GO) can be applied [3]. Generically applying GO as reflected waves, understanding the cassegrain's geometrical relationship is much easier.

As can be seen in Figure 9, the subreflector is positioned and designed to redirect the feed's rays to the main reflector. If we view the sample geometry as a transmit system, the main reflector's role is to reflect all rays from the subreflector into the direction that the antenna is pointed. These rays would ideally be parallel rays. The following sub sections describe the geometry of the main components and function in more detail. For the following sections two views will be referenced: side and top. The side view references looking at the cross section of the antenna system, see Figure 10. The top view will refer to looking down the main axis of the antenna system, see Figure 11.

2.4.1 Main Reflector Shape

The main reflector is the most easily recognized feature of the cassegrain antenna. Diameters can range from sub meter diameters [17] to tens of meters [18]. In this work the main reflector will have a diameter of 6 meters, will be circular, and follow

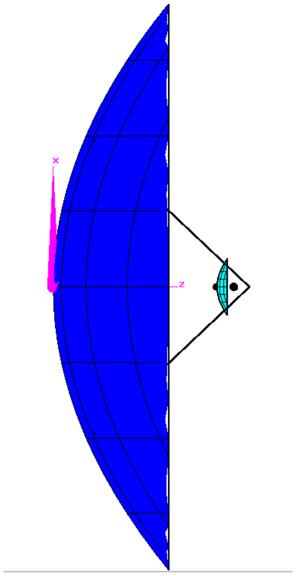

Figure 10. Cross section of the cassegrain antenna. This figure shows struts, the main reflector, and subreflector.

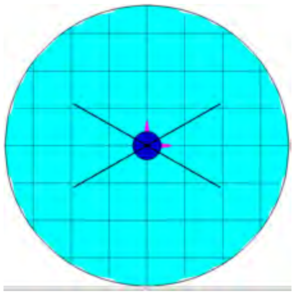

Figure 11. Looking down the main axis of the cassegrain antenna. This figure shows struts, the main reflector, and subreflector.

a parabolic contour. Ellipsoid and non-parabolic main reflectors will not be explored in this work.

As described above, the main reflector topology will be a circular disc with a parabolic contour. From the top view it will appear to be circular. This provides a significant amount of symmetry along the main axis of the antenna. From a side view the main reflector will follow a parabolic curve. Mathematically a parabolic curve follows Equation (6) where f is the focal length of the parabola and x and y are coordinates of the points which make up the parabola.

$$x = \frac{y^2}{4f} \tag{6}$$

Looking at Figure 12 it can be seen that the parabola has a couple defining features. It is defined by a vertex and focal point as well as an axis of symmetry. These features play a key role in how this shape impacts performance. The vertex's location does not alter the main reflector's performance. As seen in Equation (6), the focal length drives the overall shape of the main reflector. Focal length is the distance between the focal point and the vertex.

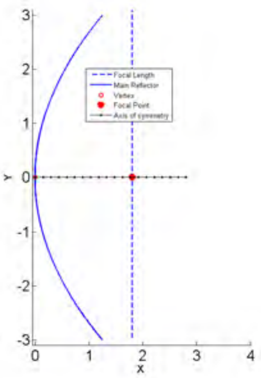

Figure 12. Parabolic curve showing the axis of symmetry, focal length, and vertex.

If we look at the parabolic curve as a reflecting surface we can see the focal point's significance. All rays entering the parabola's opening, parallel to the axis of symmetry, will be reflected to the focal point. The reverse of this is also true. If a point source is located at the focal point of the parabolic curve, all rays reflected by the parabola will be parallel. Using a parabolic curve for the main reflector's shape leads to the focal length and diameter being the main two parameters of the main reflector. With the focal length being a driving factor in correctly positioning the subreflector.

Rather than discuss focal length as a set value, it is easiest to describe this as a ratio to the dish diameter, f/d. Moving the position of the focal point changes the shape of main reflector. It is well known that changing this shape changes the performance characteristics of the antenna system [6]. Figure 13 demonstrates how changing the f/d values adjusts the main reflector shape.

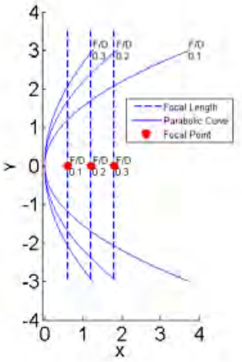

Figure 13. Example of how $\frac{F}{D}$ changes alter the shape of the curve.

Notice how decreasing the f/d elongates the shape and pulls the focal point into the "mouth" of the parabola, while increasing the f/d appears to flatten the curve and pulls the focal point external to the parabola's opening. This relationship impacts the positioning and relative angles for the struts and subreflector. With regard to this work, the parametric equation and determining the focal length will be critical. The plan for this work is to use a pre-made simulation software therefore derivations for PO and UTD are not required.

2.4.2 Subreflector Shape

Like the main reflector, the subreflector is easily identified. The size of the subreflector is dictated by the goals and application of the system. Subreflectors need to be small enough to minimize blockage but large enough that it reflects as much energy as possible from the feed. Correct positioning and shaping of the subreflector is critical to having the system work correctly. As discussed in Section 2.4.1, all rays need to appear as coming from the focal point of the main reflector. This means that all rays reflected from the subreflector need to appear as though they were emitted from the focal point of the main reflector.

The shape of the subreflector for this work will be circular from a top down point of view and hyperbolic in cross section. As with the main reflector, this geometry promotes a significant amount of symmetry but is not required. Mathematically the hyperbolic curve follows Equation (7).

$$x = a\left(\sqrt{1 + \left(\frac{y}{b}\right)^2} - 1\right) \tag{7}$$

Where x and y are local coordinates for the hyperbola, and a and b are parameters of the hyperbola. The hyperbolic curve is further defined by the values c and e. The focal point of the hyperbola is defined by c and e is the eccentricity of the curve.

$$a^2 + b^2 = c^2 \tag{8}$$

$$c = f_{hyp}/2 \tag{9}$$

$$e = c/a \tag{10}$$

$e > 1$ for a hyperbolic curve

$$\frac{x^2}{a^2} - \frac{y^2}{b^2} = 1 \tag{11}$$

Using Equation (8)-Equation (11) one can define out the exact shape and position of the hyperbolic curve for the intended application. Aligning the focal points of the hyperbolic curve and the parabolic curve is necessary in order to make reflections from the subreflector appear as though they originate from the focal point of the main reflector. This adjustment can be accounted for by modifying Equation (7) into Equation (12).

$$x = a\left(\sqrt{1 + \left(\frac{y}{b}\right)^2} - 1\right) + O \tag{12}$$

Where O is the offset value. Determining this value of O depends on the focal point of the feed, eccentricity of the subreflector, and focal point of the main reflector. Figure 14 shows a pair of hyperbolic curves and highlights how the parameters of the hyperbola are referenced. In this figure the two curves are centered at 0,0. The value a is the distance from the origin to vertex of the hyperbolic curve, b is the distance from vertex to the asymptote, and C is the distance from the origin to each focal point. Point f and f' represent the focal point and a "mirrored" or virtual focal point respectively.

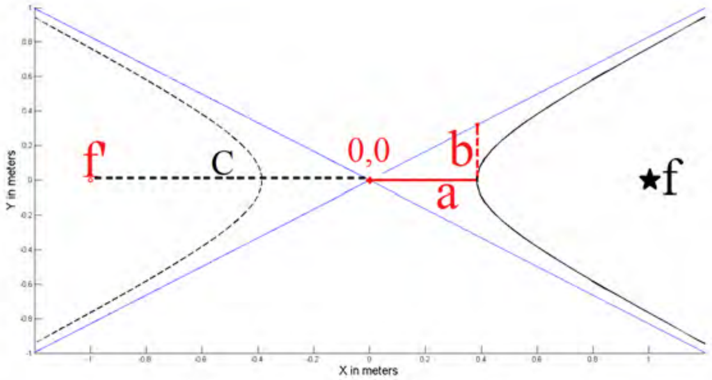

Figure 14. Hyperbolic curve with asymptotes.

Let the point f' emit a series of rays across the face of the hyperbolic curve with focal point f. The reflection of these rays will appear to originate from point f. As with the parabolic curve, deriving this geometric relationship is outside of the scope of this work. However, this is a key feature which allows the cassegrain antenna to function correctly. Aligning the focal point of the subreflector with the focal point of the main reflector is critical. Further aligning the focal point of the feed with the virtual focal point of the subreflector is also critical.

In the example provided, allowing f' to be the focal point of the feed and f to be the focal point of the subreflector leads to the geometrical relationships shown in Figure 16. In this figure it is shown that the offset, O, needed for Equation (12) becomes $c + a$.

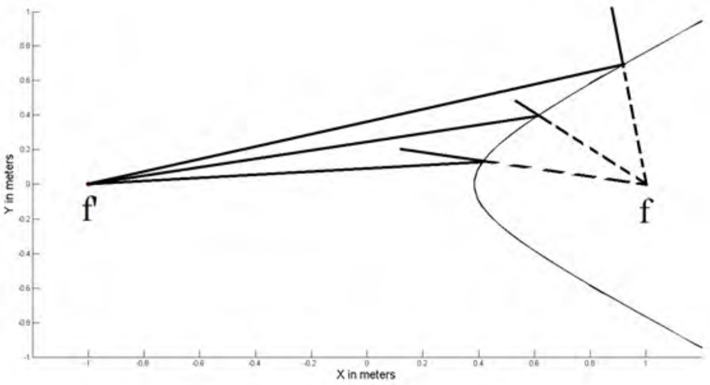

Figure 15. Diagram showing Reflections from a hyperbolic curve.

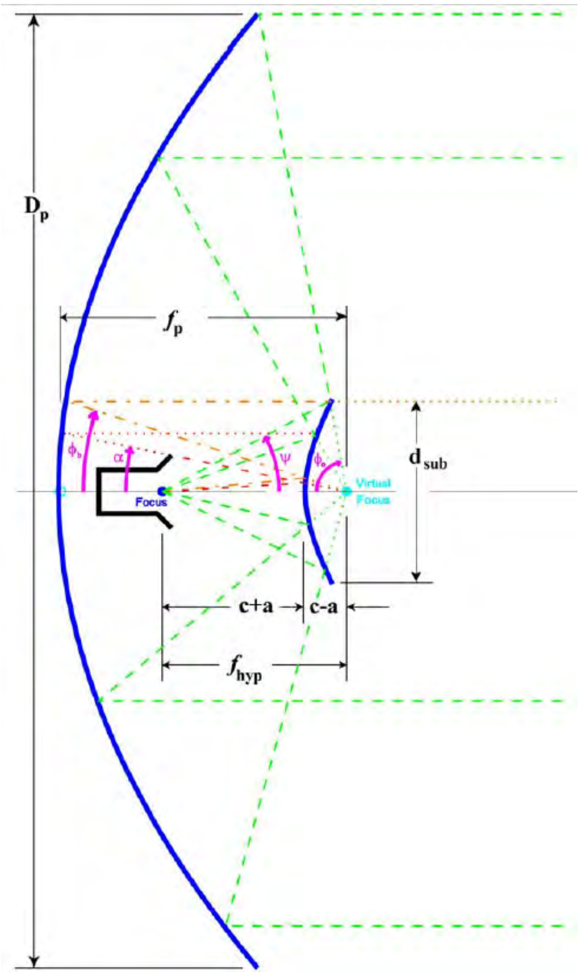

Figure 16. Hyperbolic subreflector positioning [3].

The offset value shown can also be seen in Figure 14. Defining the hyperbolic curve with an offset value allows for an easy alignment of focal points between the main reflector and subreflector. As previously mentioned, the alignment of these focal points is critical to the positioning of the subreflector. Proper positioning of the subreflector then becomes a function of the parameters c and a. Equation (10) shows that ratio of these two is the eccentricity of the subreflector.

Eccentricity of the subreflector for a traditional cassegrain antenna is always greater than 1. Increasing the eccentricity can be thought of as opening up the shape. Figure 17 shows this relationship.

Changing the eccentricity is changing the ratio $\frac{c}{a}$. As discussed, c and a are critical to the positioning of the subreflector, which leads to the eccentricity being a critical parameter of the subreflector. Another critical parameter of the subreflector is the diameter. With a traditional cassegrain antenna, the subreflector will be positioned in front of the main reflector. This configuration creates a blockage of the main beam. In simplest terms, this blockage creates a sort of “hole” in the main beam.

Obviously the blockages could be removed if the subreflector and feed were to placed off axis from the main reflector. However, that configuration is not being explored in this work. There is a proposed configuration for minimum blockage[2].

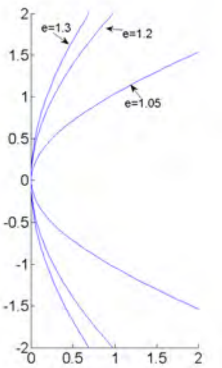

Figure 17. Varying eccentricity for a hyperbolic curve.

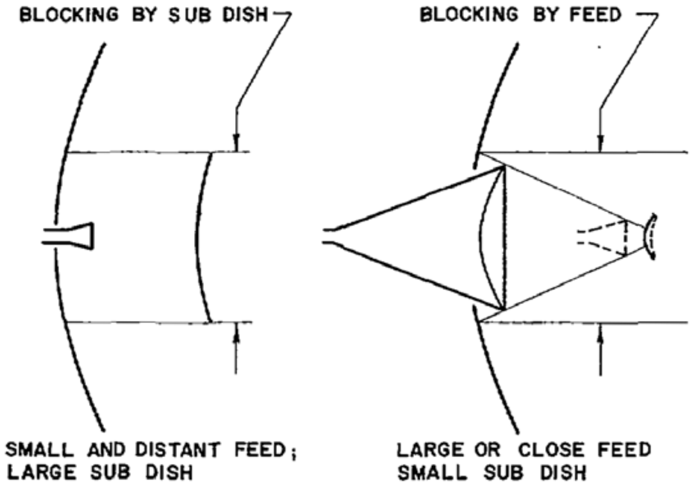

Figure 18. Blockages by the feed and subreflector [2].

The minimum blockage condition is determined by the blockage source. In some applications the feed will be the source, and in others the subreflector will be.

Figure 19 shows it is possible to keep the blockages limited to only that of the subreflector. The minimum blockage conditions are shown in Equation (13). This relationship says that the ratio of the main and subreflector focal lengths should be roughly equal to the ratio of feed diameter to the subreflector diameter, and these

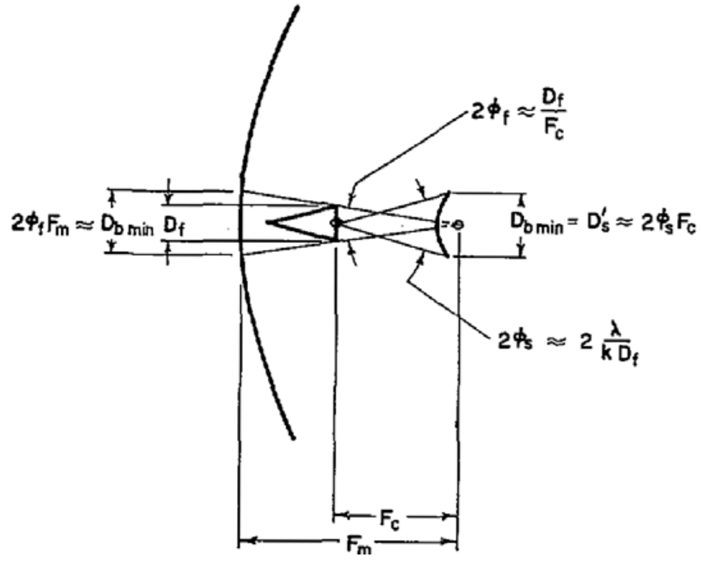

Figure 19. Minimum blockage condition [2].

two values should be roughly equal to the ratio of maximum angles between the focal points and the edge of the feed and subreflector [2].

$$\frac{f_c}{f_m} \approx \frac{1}{2}\frac{kD_f^2}{f_c\lambda} \approx \frac{D_f}{D_s'} \tag{13}$$

Minimizing the blockage from the subreflector while maximizing the amount of energy reflected from the feed to the main reflector is the key to optimizing the subreflector. This leads to the key parameters of the subreflector being its diameter, eccentricity, and positioning.

2.4.3 Feed Geometry

The role of the feed in the cassegrain antenna is to illuminate the subreflector. Horn style antennas are the traditional feed's for dual reflector antennas [19]. In this work the actual configuration of the feed will not be considered. The main concern is what the feed pattern looks like. This can be described with Equation (14).

$$\frac{e^{-A\left(\frac{\psi}{\psi_0}\right)^2}[cos^N\left(\frac{\pi\psi}{2\psi_0}\right)] + C}{1 + C} \tag{14}$$

Equation (14) is provided as the governing equation for the feed pattern used in the software SATCOM. In this equation ψ_0, A, C, and N are all curve parameters. For this work A and C will be held at 0 and ψ_0 will be held at π. This leads to equation Equation (15). Where ψ is the angle from the main axis and N is a curve parameter which allows for the adjustment of the beamwidth of the feed.

$$cos^N\left(\frac{\psi}{2}\right) \tag{15}$$

Relating the feed pattern to the subreflector it can be seen in Figure 16 that the angle Ψ is the angle between the feed's focal point and the edge of the subreflector. This value will change as a function of diameter of the subreflector and the distance between subreflector and the feed's focal point. Since the subreflector is illuminated by the main lobe of the feed antenna, the power imparted on the surface of the reflector will change. Edge taper is the term for the power level of the feed at angle Ψ. Adjusting the edge taper allows for more or less overshoot of the subreflector. Overshoot is how much energy from the feed is not reflected by the subreflector.

Edge taper turns out the be a function of the feed geometry and how the feed's beam pattern relates to the subreflector's dimensions. In order to determine what the edge taper is for a set geometry, the angle Ψ needs to be found and then compared against the feed pattern plot.

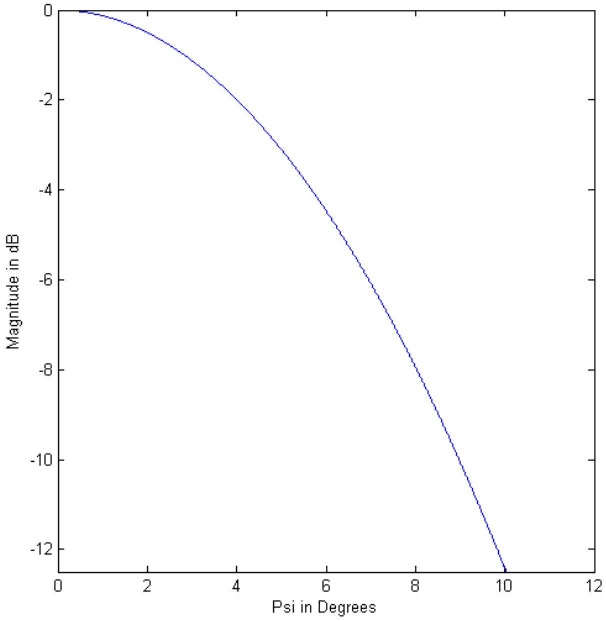

Figure 20. Sample Feed pattern with N=100.

In Figure 20 the curve shows how the feed pattern changes as a function of ψ. In this example, if the subreflector formed an angle of 12° for Ψ, then the edge taper would be approximately -12.5 dB. With regard to the feed geometry, this concept of an edge taper is the key parameter.

2.4.4 Strut Geometry

As discussed in Section 2.4.2, the subreflector needs to be located properly to align the focal points. In larger antennas, struts are typically used to support the subreflector. In this work the strut geometry will utilize 4 struts which are connected to the edge of the subreflector rather than attaching to the face of the subreflector. The angle that these struts form with the main axis of the antenna will referenced. This angle can be found using trigonometry.

Attaching the struts to the edge of the subreflector allows this point to act as a sort of pivot point. The distance from both the main axis and origin to the pivot point will remain static as the strut angle is changed. The distance from the origin to where all 4 struts connect together will change as a function of strut angle. There are at least two different approaches which can be used to determine these connection points and strut angles. The first approach is assume a strut angle and then calculate the connection points. The second is to assume connection points on the main reflector and then solve for the strut angle. Both approaches will be applied in this research since each has its advantages and disadvantages. Regardless of the approach, a 3-D geometry needs to be assumed. A side view of the strut geometry was shown in

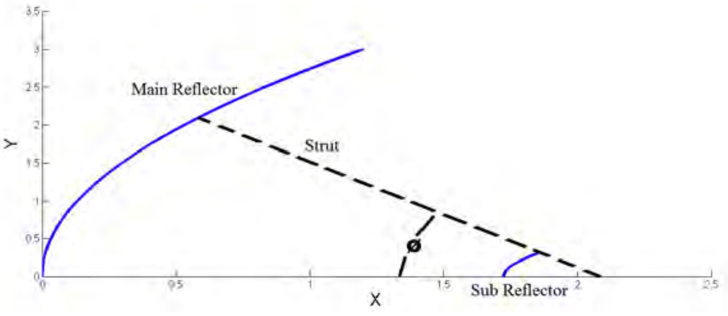

Figure 21. Strut angle is referenced to the main axis.

Figure 21. Looking at the struts from a top view, the strut configuration of interest is shown in Figure 22.

Since the sub and main reflector's are both circular, the strut geometry can be broken down into two pieces. The two pieces consist of a top view and side view geometry. Before assuming the top view strut separation angles, it is easiest to assume all of the struts are separated by 90 degrees. This allows for a simplification in calculating the strut lengths and angles. Regardless of the strut separation angle, the struts will all be equal length and their angle with respect to the main axis will not change. Starting with this simplified side view geometry, finding the key connection points means applying some trigonometry. Before getting to equations to solve this problem, it is assumed that the parameters for both reflectors are known. These will be vital to actually finding values for the struts.

Starting with assuming a strut angle and the connection point to the subreflector, the geometry in Figure 23 is formed. The curves for the main and subreflectors have been removed since they clutter the image with excessive lines. This provides two right triangles which can be used to start solving key values.

Something to note is that in order to locate these struts in 3 dimensions, a coordinate system needs to be applied. In this application the Z axis will be the main axis of the antenna system and X and Y will be normal to each other and Z. Looking

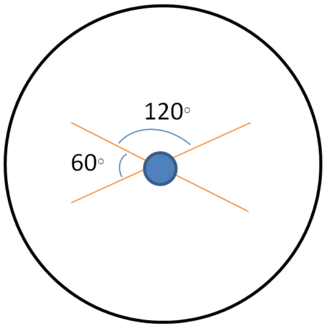

Figure 22. Strut angles referenced to each other.

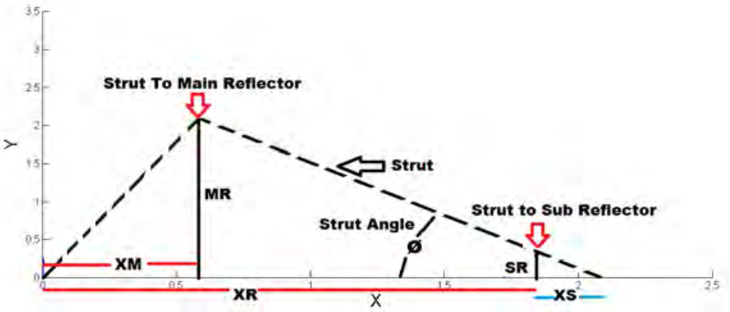

Figure 23. Side view geometry for locating struts.

down from the top view of the antenna will be the X and Y coordinates. In order to place the struts, starting and ending points for each coordinate needs to be found. Allowing all of the struts to terminate at a common point simplifies this problem. This leads to needing to find a starting X,Y, and Z. The ending values for X and Y will be 0, but an ending value for Z will need to be found. Solving the triangles in Figure 23 will allow for finding starting and ending Z values.

M_R is the radius from the main axis to where the strut contacts the main reflector.

S_R is the radius of the sub subreflector.

X_M is the distance from the base of the main reflector to the line normal of the strut to main reflector connection point.

X_R is the distance from the base of the main reflector to line normal to the edge of the subreflector.

X_S is the distance from line normal to edge of the subreflector to the common connection points of the struts.

Summarizing this, X_M will be the starting Z value and X_R+X_S will be the ending Z value. M_R is used to determine X and Y coordinates from the top view. Solving the triangles in fig. 23 leads to equations (16) – (20).

$$X_S = \frac{S_R}{tan(\theta)} \tag{16}$$

$$X_{tot} = X_R + X_S \tag{17}$$

$$M_R = \frac{X_{tot} - \frac{M_R^2}{4F}}{cot(\theta)} \tag{18}$$

Rearranging and solving for M_R leads to

$$M_R = -2Fcot(\theta) \pm 2F\sqrt{cot(\theta)^2 + \frac{X_{tot}}{F}} \tag{19}$$

Using MR solving for XM is simply

$$\frac{M_R^2}{4F} \tag{20}$$

With the start and end Z values found locating the starting X and Y coordinates is done from the top view. In the top view, using M_R as the radius from the origin to the end of the strut simplifies work to be done. This starts by breaking down the strut separation angles into values relative to the X and Y axis. Using basic trigonometry it is known that the XY coordinates for each strut can be broken down as $X = Rcos(\theta)$, $Y = Rsin(\Theta)$ where $R = M_R$ in this application. Figure 24 shows how θ is referenced. Table 2 displays how these angles relate to specific struts.

Alternatively, the strut angle can be found assuming a specific radial length from the main axis to the connection point of the main reflector. This leads to solving for the angle theta as a function of the height M_R. In order to solve this problem figure

Table 2. Angles used for calculating X and Y positional values.

Strut 1	30°
Strut 2	150°
Strut 3	210°
Strut 4	330°

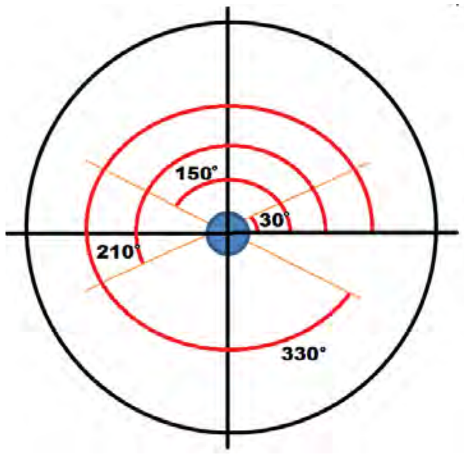

Figure 24. Geometry used for locating the struts.

Figure 23 is modified to be that in Figure 25.

In Figure 25 another triangle has been formed. M_R is still the distance from the main axis to the main reflector. A is the angle that is formed between the main axis and a line from the strut reflector connection point to the origin. S_{RE} is a line from the origin to the edge of the subreflector. C is the angle between that line and the main axis. B is the difference in angles between A and C. This geometry allows the application of law of cosines to solve for S_L and then law of sines to solve for D. Theta is solved by subtracting the values of angle A and D from 180 since all angles in a triangle must add up to 180 degrees.

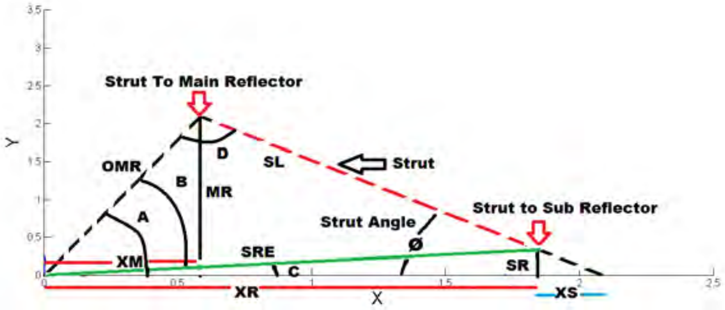

Figure 25. Geometry used for solving the strut angle.

$$A = tan^{-1}(\frac{M_R}{X_M}) \tag{21}$$

$$C = tan^{-1}(\frac{S_R}{X_R}) \tag{22}$$

$$B = A - C \tag{23}$$

$$S_L = \sqrt{O_{MR}^2 + S_{RE}^2 - 2O_{MR}S_{RE}cos(B)} \tag{24}$$

$$D = S_{RE}\frac{sin(B)}{S_L} \tag{25}$$

$$\theta = 180 - D - A \tag{26}$$

$$X_S = \frac{S_R}{tan(\theta)} \tag{27}$$

X_M would be the Z start value and $X_R + X_S$ would be the Z end value. The starting locations for X and Y are found using Table 2 and trigonometry.

2.5 Simulation Software

Numerical analysis could be used to determine field strengths and beam patterns from the antennas. In this work the antenna being analyzed is electrically large. This limits the numerical techniques to asymptotic techniques and potentially a method of moments technique. There are a couple of computational software packages available which utilize these techniques. CST and GRASP are two commonly used software packages. As discussed in Chapter I, this work was spawned from an analysis on another cassegrain antenna. The previous work used a software package called SATCOM which was developed at Ohio State University (OSU).

CST has modules for doing asymptotic analysis and method of moments analysis. This software suite allows the user to build the geometries in a flexible development environment where the components can be parameterized. Using a parameterized model in CST will allow the user to perform successive simulations where small changes can be quickly analyzed. CST can provide near and far-field simulation results. Early attempts at using CST to model the 10 m antenna did not go well, and it was realized that an accurate feed model would be needed in order to have confidence in the results.

GRASP uses asymptotic techniques to quickly analyze electrically large reflector antennas. The software provides a user friendly interface for quickly designing various geometries. Like CST, GRASP provides a means of automating parameter changes to analyze how parameter changes impact the antenna system's performance. GRASP can provide near and far-field simulation results. For this work only the student edition of GRASP is available. This limits the capabilities of GRASP significantly. In the student edition, struts are not able to be included, near field data is not able to be collected, and parameter sweeps are not available.

SATCOM is an older software which also uses asymptotic techniques for analyzing reflector antennas. This software provides an intuitive GUI for generating the dual reflector geometries. Unlike the other two software packages, performing parameter sweeps cannot be readily done without building multiple models. SATCOM only provides far-field data results.

In this work a combination of GRASP student edition and SATCOM will be used. SATCOM was previously used to model a 10 m cassegrain antenna, and the results were generally accepted as accurate. Results from GRASP and SATCOM will be compared to highlight the impacts of not including UTD. Both software packages have been used and accepted in the community as providing valid results [20, 4, 21, 6, 22]. Generally speaking, the authors in the papers cited the simulation results as acceptable as compared to the measured results.

2.6 Accepted Design Principals

Overall, the design of any antenna will come down to budget, size constraints, and performance requirements. With regard to the cassegrain antenna the main reflector diameter will drive many of the further design choices. The main reflector has 2 key parameters: the diameter and the focal length to diameter ratio f/d. Typical values for f/D_m fall within the range of 0.25 to 0.85. It has been asserted that a larger f/d reduces cross polarization but increases strut length [11].

With the main dish diameter set, the subreflector diameter can be chosen. Smaller values for the ratio of the subreflector to main reflector diameter ratio lead to lower side lobe levels, but larger values are asserted to have high power handling [6]. The typical value is for a D_s/D_m is $\leq$0.1, which keeps blockage to a minimum [11].

Edge taper values are targeted to be between -10 and -15 dB[11]. These values minimize spillover and helps keep proper illumination of the subreflector. In practice the subreflector parameters are adjusted to the intended feed. The feed pattern would be known and the eccentricity of the subreflector would be derived from the feed pattern, diameter of the subreflector, and focal lengths of the main reflector and feed[12].

Table 3. Typically accepted design parameter values.

Parameter	**Value**
F/D	0.25 to 0.85
Ds/Dm	$\leq$0.1
Edge Taper	-10 to -15 dB
Eccentricity	Derived from feed and subreflector

III. Methodology

3.1 Preamble

Characterization of the 6 m cassegrain antenna will begin with looking at the previously characterized 10 m cassegrain antenna. This will allow for identifying a set of starting parameters and also a comparison point for the overall performance. Since the optimum parameters for a 6 m cassegrain are assumed to be different than a 10 m antenna, each parameter will be varied to determine the impacts. This detailed study will provided a sensitivity analysis resulting in a performance range.

Each of the parameters will be evaluated for its contribution to peak directivity, main lobe beamwidth, and side lobe contribution. Strut location and geometry will also be evaluated for these attributes, and will also include an identification of far side lobe contributions; namely peak location and relative level. All sensitivity analysis will be done through simulations and analysis of the results.

The simulation suites discussed in Section 2.5 were previously used to simulate the 10 m cassegrain antenna. After using each of these it was determined that due to availability and functionality, SATCOM would be used for the far field simulations and GRASP student edition would be used to cross check the results from SATCOM. The previous 10 m simulation results were generally accepted as valid. SATCOM's user interface is not clear on whether diffraction terms are used. The omission of diffraction terms reduces the accuracy of the results in various ways. GRASP includes diffraction terms in its simulations, and the results between SATCOM and GRASP will be compared. Restricting the beam pattern analysis to the main lobe and first two side lobes will also help maintain a satisfactory level of accuracy. The following sections will discuss in further detail how this analysis will be done.

3.2 Verification

As mentioned, the results from each software package will be compared against each other, and also to the previous work. This will be accomplished by extracting all of the required parameters from the previous documentation. When that documentation does not provide the necessary values, the values will be calculated or assumed as required.

Another point of comparison will be against the paper titled “Pattern Measurements of Reflector Antennas in the Compact Range and Validation with Computer Code Simulation”. In this paper the authors modeled a small cassegrain antenna using the reflector analysis code SATCOM, and measured its pattern in a compact range. The simulation results aligned well when compared against the measured results. The authors of this paper provide critical dimensions to reproduce the reflectors as well as a plot of the feed horn’s measured performance. Rather than use SATCOM to repeat this work, GRASP will be used as such struts will not be included in the simulation.

3.3 Parameter Sweeps

As discussed there will be a static configuration, and each of the parameters will be individually swept while holding the other parameters static. This will allow for an understanding of how each parameter impacts the beam pattern of the cassegrain antenna. Another benefit is that it will highlight how sensitive the beam pattern is to minor changes in each of the parameters. The outcome of each of these parameter changes will be evaluated for impact to the maximum power on the main lobe, the 3 dB cutoff of the main lobe, and the first two side lobe levels and location in degrees from the main axis. While evaluating all of these parameters, struts will not be included due to the complex nature of how the struts impact overall beam pattern.

The antenna patterns from the simulations will be varied as a function of θ and ϕ. Where θ is referenced from the side view and is the angle off the main axis. ϕ is referenced from the top view and is rotational angle. Figure 26 demonstrates how θ is referenced, and Figure 27 displays how ϕ is referenced.

Referencing the beam pattern angles in this way leads to symmetries which can be used to reduce the range needed for the simulation. In Figure 26 it is clear that there is symmetry along the main axis in θ. This can be used to limit the simulation range from -180°-180° to 0°-180°. With regard to ϕ, when the struts are not present only one angle of ϕ would be needed. If the struts are present it appears only 0° to 90° would be needed.

All of the parameters, including the struts, will be simulated across θ and ϕ as needed. Each parameter sweep value range, to include the struts, will be swept across a wider range than the typically accepted values. To conclude the characterization,

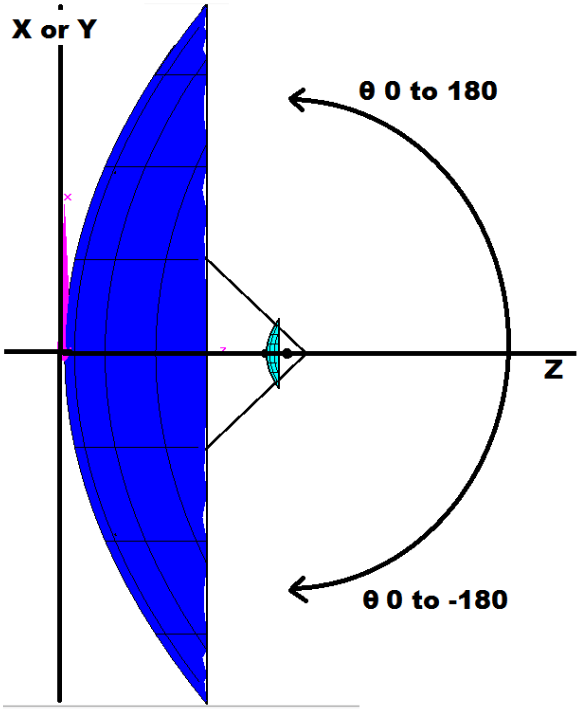

Figure 26. Shows how θ is referenced and illustrates the symmetry.

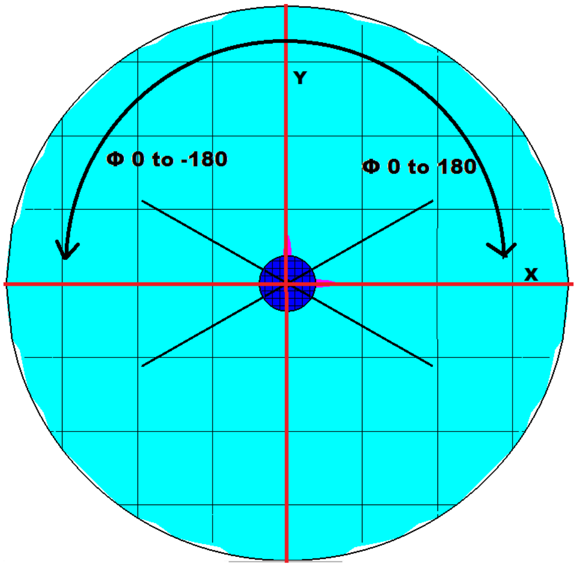

Figure 27. Shows how ϕ is referenced and illustrates the symmetry.

a comparison between the assumed values and optimized values will be completed. Each of the parameter sweeps will be discussed further in the following subsections, to include how the other parameters are impacted by changes of the parameter being evaluated.

In order to facilitate single parameters sweeps all of the other parameter values will be calculated and adjusted as appropriate to isolate the parameter being swept. Calculation of these values will use Equations (6), (12) and (15). Sweeping of the strut angles will require the calculation of the start and end location of the strut as a function of the angle of the struts.

3.3.1 Focal Length to Main Reflector Diameter Ratio

As previously discussed, the focal length to main diameter ratio drives many of the other design choices in the cassegrain antenna. Adjusting f/d ratio changes the position of the focal point of the main reflector. This change will also reposition the subreflector. As the subreflector moves relative to the feed, the apparent edge taper of the feed will change. Changing the position of the subreflector will change the relative positioning of the struts. As previously discussed, all of the other parameters will be held static.

In order to hold the other parameters static, adjustments will be made to the antenna configuration to simulate only changing the f/d value. Strut effects will be neglected as struts will not be included in the simulation. Subreflector parameters will be held static by keeping its focal points aligned with the focal point of the main reflector and feed, as well as keeping its eccentricity consistent. As the subreflector moves toward and away from the feed, the angle between the feed's focal point and the edge of the subreflector changes. This change requires the adjustment of the feed's parameters to keep the edge taper value constant. This parameter will be evaluated from an f/d of 0.1 to 0.6.

Overall, this means that the focal length will be adjusted from a value of 0.60 meters to 3.6 meters for a 6 m diameter cassegrain antenna. The typical values for f/d range from 0.25 to 0.85, which represents a focal length of 1.5 meters to 5.1 meters. While the typical value for f/d extends out to 0.85 in this work, f/d will not be extended to 0.85 due to the long focal length. Figure 28 depicts the minimum, maximum, and assumed value for the parameter sweep changes the geometry.

Figure 28 also shows how the subreflector is affected by the extremes of the f/d values evaluated in this work. Notice how the subreflector is moved toward or away from the feed. As discussed in Section 2.4.2, the alignment of the subreflector's focal points with the main reflector and feed's focal points is critical.

3.3.2 Subreflector to Main Reflector Diameter Ratio

Unlike changing the f/d ratio, changes to the diameter of the subreflector will not impact as many other parameters. As the diameter of the subreflector changes, the angle between the feed's focal point and the edge of the subreflector changes.

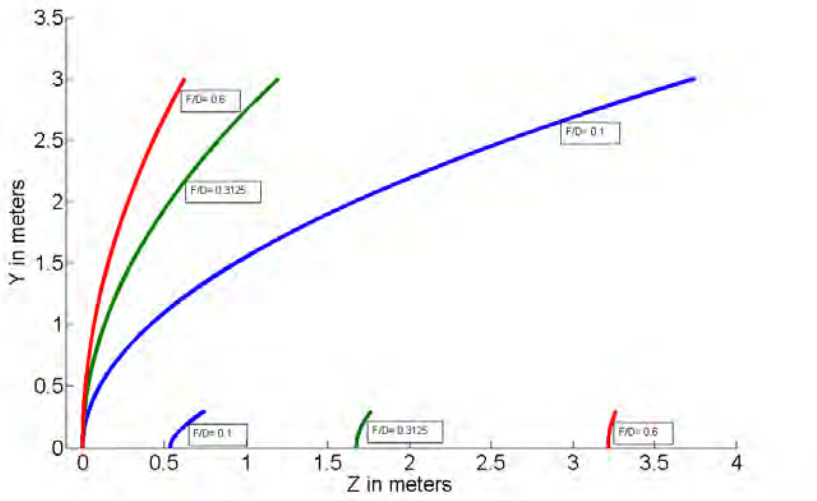

Figure 28. Displays the range of f/d, and how it changes the shape of the main reflector, and location of the subreflector.

This will require adjustments to the feed's parameters to keep the feed's edge taper consistent while the diameter of the subreflector is changed. This sweep will start at a value of 0.01 and end at a value of 0.30, which represents a minimum diameter of 6 centimeters to a maximum diameter of 1.8 meters. Figure 29 shows the maximum, minimum, and assumed values for subreflector diameter. Typically, the value for the subreflector to main reflector diameter ratio is less than or equal to 0.1 in order to minimize blockage. For a 6 m cassegrain antenna, that would represent a subreflector diameter of 0.60 m or smaller.

Figure 29 shows how the extreme ranges of this parameter sweep impact the angle between the feed's focal point and the subreflector edge. The ratio between the subreflector and main reflector's diameter is annotated as Ds/Dm and the angle between the feed's focal point and edge of the subreflector is annotated as SrA.

3.3.3 Subreflector Eccentricity

Changing the eccentricity of the subreflector is similar to changing the focal length of the main reflector. Changing this value changes the subreflector's focal length. As

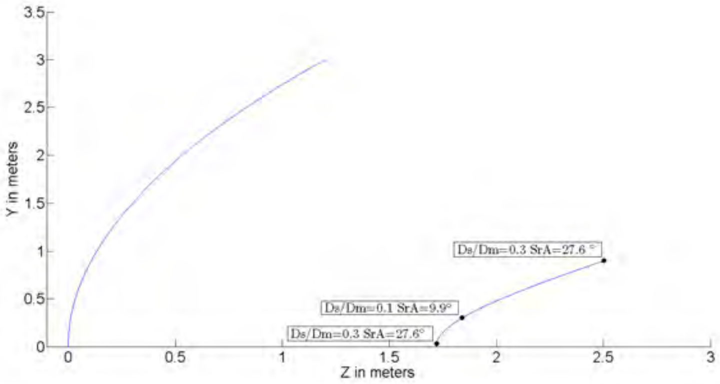

Figure 29. Displays the range of $\frac{Ds}{Dm}$, and how it changes the angle between the feed's focal point and the edge of the subreflector.

the subreflector shape changes, its vertex will need to move toward and away from the focal point of the feed to keep the main and subreflector's focal points aligned. While the subreflector's shape is being changed, the diameter of the subreflector will not change. Holding the subreflector's diameter the same while it moves toward or away from the feed's focal point will again change the angle between the edge of the subreflector and the focal point of the feed. This change will necessitate the adjustment of the feed's parameters to maintain a consistent edge taper. This parameter will be swept from a value of 1.05 to 3.0. The typical value for this parameter is derived based on the feed's edge taper, subreflector diameter, and the main reflector f/d value.

Figure 30 shows how this parameter sweep changes the cassegrain antenna's geometry. Notice, as the the subreflector eccentricity increases it appears to flatten out and its vertex moves toward the feed's focal point, while a lower eccentricity appears to elongate the subreflector. The angle between the feed's focal point and edge of the subreflector will also increase as the subreflector eccentricity is increased. This is annotated as SrA in the plot.

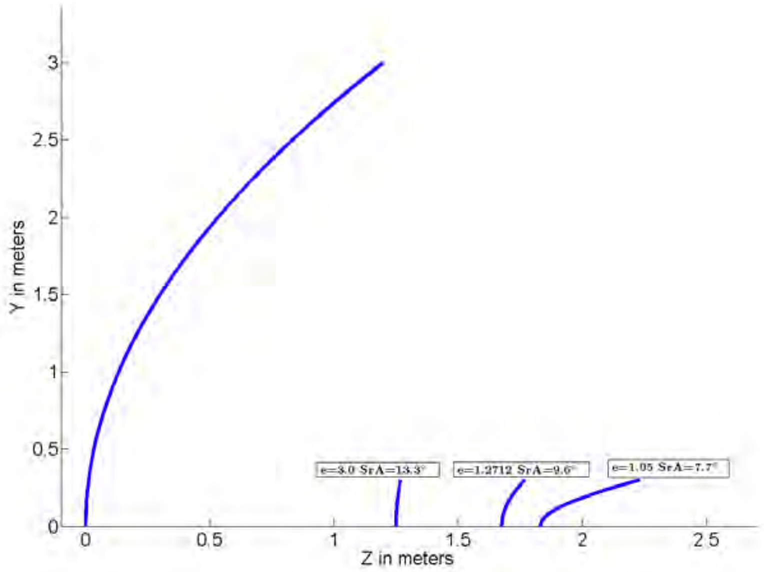

Figure 30. Displays the range of eccentricity, and how it changes the angle between the feed's focal point and the edge of the subreflector.

3.3.4 Feed Edge Taper

In the previous sub sections, the feed edge taper was held consistent while the parameter being evaluated was changed. To understand how the feed's edge taper impacts the performance of the antenna, it will be used as a sweep parameter. Changing the parameters of the feed does not require the adjustment of any other parameter. This parameter will be swept from a value of 0 dB to -30 dB, while the typical range is -10 dB to -15 dB. As with the other parameters increasing this range helps highlight the behavior of the antenna pattern at extreme ranges.

Figure 31 shows the extremes of this parameter sweep and the assumed value. Note how the beam pattern of the feed changes as a function of edge taper. In this plot the absolute minimum was not plotted. An edge taper of -0dB would indicate that there is no change in power level from the center of the main lobe to the edge of the subreflector. Plotting this would simply be the line at 0dB across all angles of ψ. Rather than include this line which would likely be overlooked an edge taper of -1dB

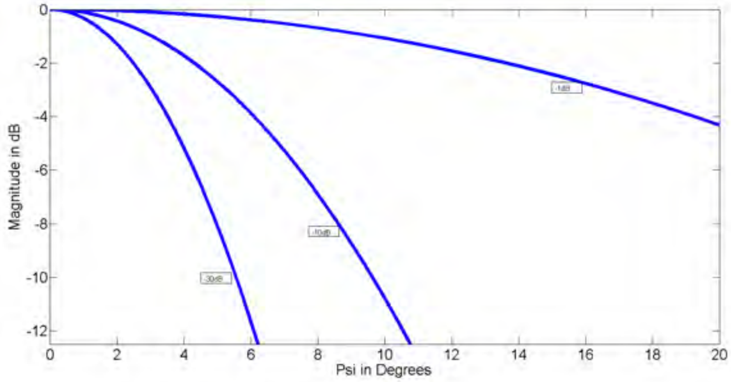

Figure 31. Displays the range of edge taper values.

was used. The edge taper values shown in Figure 31 are referenced to the assumed source to subreflector edge angle of 9.6°.

3.3.5 Strut Angle

Supporting structures for the subreflector are referred to as struts. The location and geometry of these struts will impact the performance of the antenna. In this work the subreflector will be supported by 4 struts. Each strut will be located such that it is on the subreflector's edge and extends to the surface of the main reflector. From a top down view, pairs of struts will be separated by 120 degrees, and the struts in each pair will be separated by 60 degrees. Figure 32 shows this configuration. Each strut will be assumed to have a circular cross section with a radius of 1 cm.

The strut angle with respect to the main axis will be varied from 5 degrees to 78 degrees. Figure 33 shows how this angle is referenced. Each strut will connect at a common point along the main axis of the antenna and terminate at the surface of the main reflector based on the strut angle and separation angle required for each strut. These points will be calculated based on the equations in Section 2.4.4.

In order for the calculations to locate the start and end point for each strut, both reflectors need to be defined geometrically. As in previous sections, the assumed values

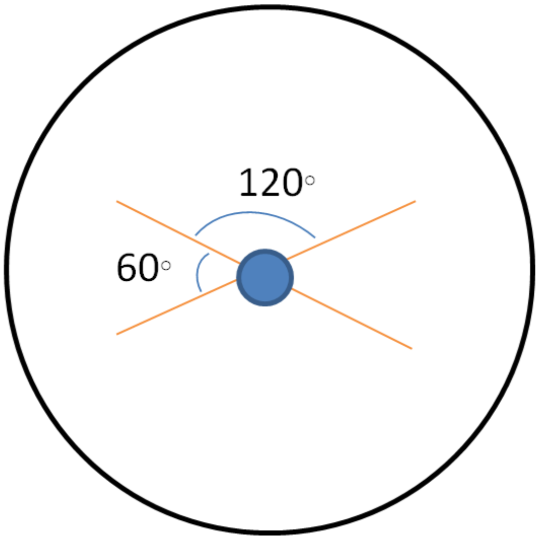

Figure 32. Assumed strut configuration from a top down view.

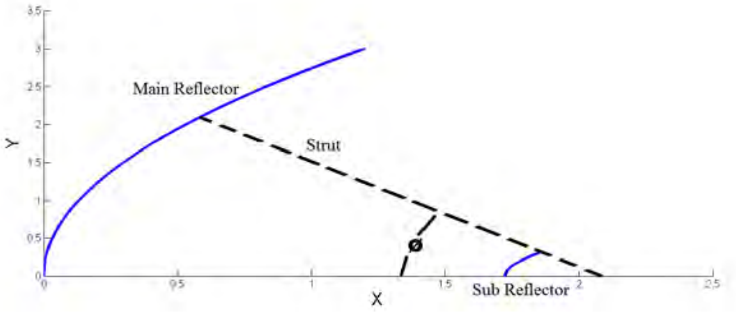

Figure 33. The strut angle parameter will be referenced to the main axis of the antenna as shown.

will be used and will not vary during this parameter sweep. With the geometry of the main and subreflector being held static, the maximum of extension of the subreflector also becomes static. Using the circular symmetry of the cassegrain antenna, one can find the maximum extension of each strut with respect to the vertex and connection point to the main reflector, and the total length of the strut.

3.4 Beam Pattern Comparison

A performance band can be established using the data from the sensitivity analysis. Simulations using the maximizing values for each of the parameters will be compared against the assumed parameter values. The lower end of the performance band can simulated using minimizing values within the typical values for each parameter. Each of the patterns can be compared based on main lobe peak power, 3dB beam width as well as side lobe performance. Each of these 3 patterns will use the assumed strut angle.

IV. Results and Analysis

4.1 Preamble

This chapter will detail the data resulted from the methodology described in chapter 3. The focus of this chapter is to detail the antenna parameters used and the analysis applied for the final results. Repeat work for the 10 m antenna will be covered. Which includes the comparison of previous work against the new simulations using the assumed parameters. This chapter will conclude with the presentation and analysis of the work done for the 6 m antenna, to include the comparison between GRASP and SATCOM, as well as results for the sensitivity analysis. A short discussion on the analysis method for the results will be provided in each section.

4.2 Verification

GRASP was used to repeat the work from [4]. In this recreation of the work, struts where omitted and the feed horn's performance was estimated based on the measured results displayed in [4]. Table 4 provides the parameters used in the verification plots. All results were normalized to mimic the original work's presentation of the results.

Table 4. Repeat of OSU simulation using GRASP.

Parameter	**Values**
Frequency	11 GHz
Polarization	Linear
Feed Location	22.3" from Focal Point
Edge Taper	-10 dB at 20°
Dm	96"
$\frac{F}{Dm}$	0.5 (C)
$\frac{Ds}{Dm}$	0.37 (C)
SR Vertex	22.3" from Feed
Eccentricity	1.58 (C)
Strut Angle	omitted

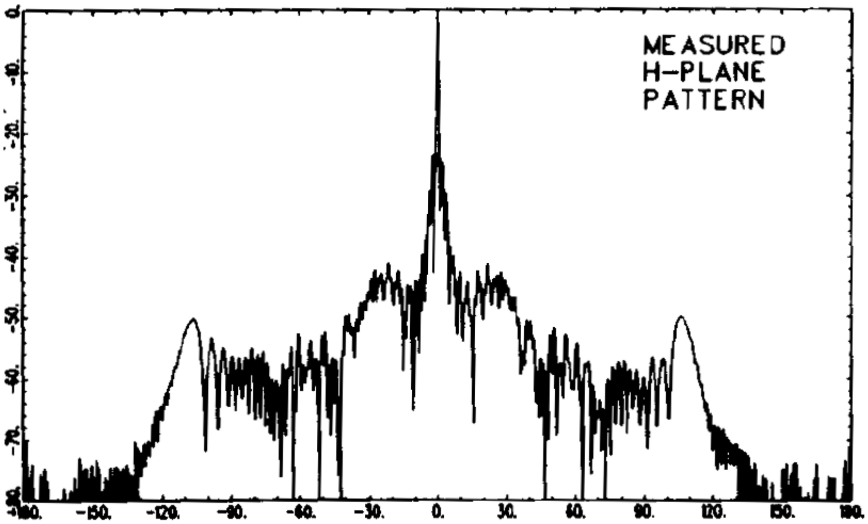

Figure 34. OSU's original results for the 96" cassegrain -180° to 180° [4].

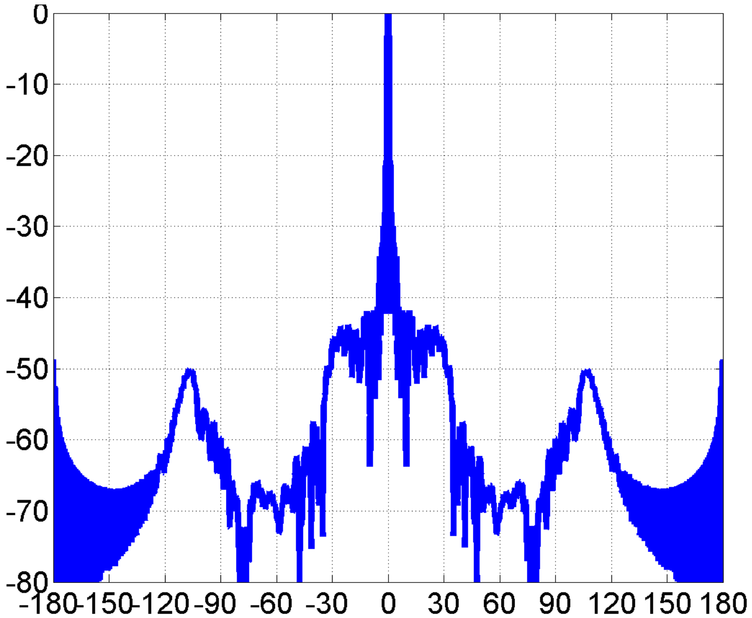

Figure 35. GRASP results for the 96" cassegrain -180° to 180°.

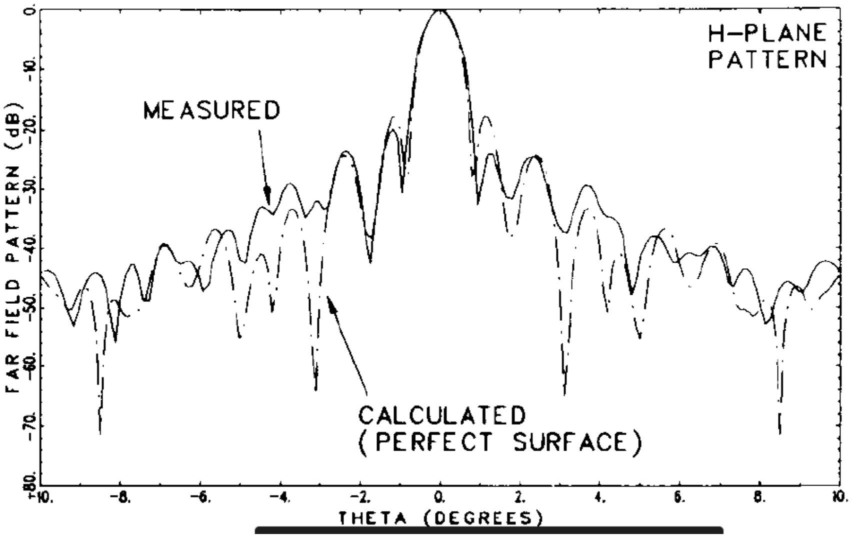

Figure 36. OSU's original results for the 96" cassegrain -10° to 10° [4].

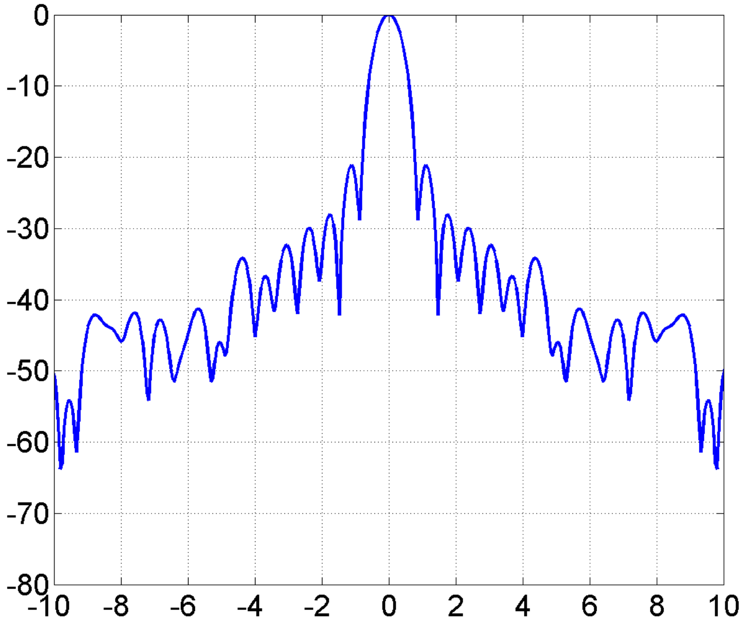

Figure 37. GRASP results for the 96" cassegrain -10° to 10°.

After simulation of the 96 inch cassegrain antenna in GRASP, the results were normalized and plotted for comparison against the original results. Comparing the -180° to 180° plots against one another, the two agree reasonably well considering struts were omitted and the feed was significantly simplified. Comparing both plots from -10° to 10° reveals additional information. In the Ohio State University (OSU) paper, the first side lobe was reported to be at 1.14° θ, and appears to have a level of approximately -20 dB. The GRASP results show a first side lobe at 1.11° at a level of -21 dB. Given the simplified feed model and a lack of struts, the results agree reasonably well. A significant take away from this simplified modeling is that, without a very detailed feed description, all of the results from this work are only to be considered estimates.

4.3 10 m diameter results

Previously the 10 m diameter cassegrain antenna was simulated in SATCOM. These results were accepted as good data and the parameters used in these simulations will be used as the assumed values, for the 6 m cassegrain antenna. In an effort to confirm and verify the assumed values the 10 m diameter antenna was simulated in both GRASP and SATCOM. SATCOM simulations were done both with and without struts. The results including struts are compared against the old data, and the results without struts are compared against GRASP. As previously mentioned, the student edition of GRASP does not provide the option to simulate with struts. The first step to conducting this work was to use the old parameters provided to derive the full set of parameters required for each of the software packages.

From Figure 38 it can be seen that most of the required parameters for simulating the antenna were provided. Table 5 provides the full list of parameters. Values which were not provided directly are annotated as (A) for assumed and (C) for calculated,

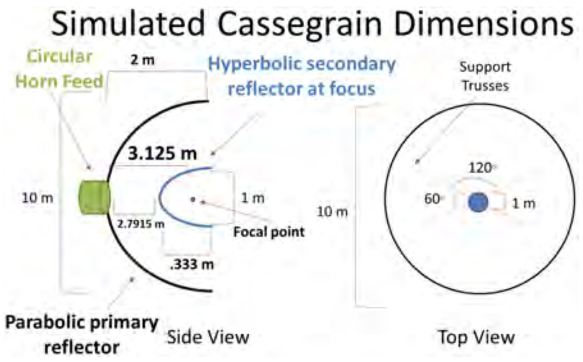

Figure 38. Parameters as presented in the previous 10 m characterization work.

values which do not include annotation were extracted directly from the material provided.

The ratios of $\frac{F}{Dm}$, $\frac{Ds}{Dm}$, and Eccentricity ($\frac{c}{a}$) were calculated. The polarization used was assumed based on discussions with the organization who requested the initial characterization work. The edge taper value was chosen from the typical range of -10dB to -15dB. -10dB was chosen since it should be the worst case value based on spill over. Spill over is the amount of energy which passes by the sub reflector. The assumption for the strut angle was made by assuming the strut would contact the surface of the main reflector at roughly 1/2 of its radius.

Assumed values were not used in the initial comparison run for the comparison

Table 5. Table of assumed parameters based on the previous work.

Parameter	Values
Frequency	10 GHz
Polarization	Right Hand Circular (A)
Feed Location	Main Reflector Base
Edge Taper	-10 dB (A)
Dm	10 m
$\frac{F}{Dm}$	0.3125 (C)
$\frac{Ds}{Dm}$	0.1 (C)
SR Vertex	2.7915m
Eccentricity	1.2712 (C)
Strut Angle	39.26° (A)

Table 6. Table of previous used simulation parameters.

Grid size	0.25 wavelengths
Frequency	9,10,11 Ghz
θ	0° to 180° by 0.025°
ϕ	0° to 90° by 10°

of the old SATCOM data to the new SATCOM data. Errors were made during the initial simulation setup, and were later corrected for subsequent simulations. The values as simulated and compared are shown in Table 7.

The old data plot was provided in a MATLAB figure. Scripts were written in MATLAB to load and plot the data from MATLAB. Figures 39 to 41 show the old data plotted against the new data from in the range of 0° θ to 10° θ at ϕ angles of 0°, 40°, and 90°. Table 9 is a table which compares the main lobe directivity, beamwidth, and first side lobe performance.

Clearly the two data sets do not line up within the first 10°, and the main lobe is showing nearly a 3 dB difference. Looking at more angles of θ reveal even more discrepancies. Figure 42 appears to show that the two simulations start to agree in the 20° to 40° range for θ, but then deviate from each other starting around 55° θ. Another major thing to note between the two data sets is the alignment of the lobe

Table 7. Table of parameters initially used for replicating the 10 m antenna results.

Parameter	**Values Used**	**Deviation**
Frequency	10 GHz	0
Polarization	Right Hand Circular (A)	0
Feed Location	Main Reflector Base	0
Edge Taper	-11.52 dB (A)	-1.5 dB
Dm	10 m	0
$\frac{F}{Dm}$	0.3125 (C)	0
$\frac{Ds}{Dm}$	0.1 (C)	0
SR Vertex	2.7915m	0
Eccentricity	1.2712 (C)	0
Strut Angle	38° (A)	1.26 °

Table 8. Simulation results of the repeated 10 m simulation compared to the previous data 0° and 40° results.

	Old ϕ 0°	**New ϕ 0°**	**Old ϕ 40°**	**New ϕ 40°**
Main Lobe Max	55.37	58.51	55.37	58.51
Half Power Beam Width	0.2°	0.2°	0.2°	0.2°
First Side Lobe Max	33.03	33.21	33.04	33.29
First Side Lobe Location	0.35°θ	0.35°θ	0.35°θ	0.35°θ

Table 9. Simulation results of the repeated 10 m simulation compared to the previous data 90° results.

	Old ϕ 90°	**Newϕ 90°**
Main Lobe Max	55.37	57.92
Half Power Beam Width	0.2°	0.2°
First Side Lobe Max	32.83	33.37
First Side Lobe Location	0.35°θ	0.35°θ

caused by the struts. The difference in the strut lobe can also be seen in Figure 42. The strut lobe in this figure appears at roughly 42° for the new data and 90° for the old data.

An alternate way to look at this strut data is by plotting the beam pattern as a 2-D image with a color map. Viewing the data in this way allows for quickly identifying

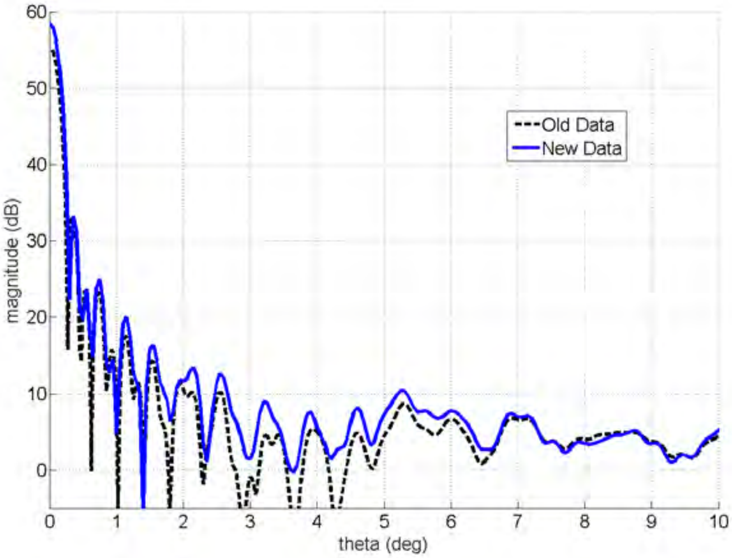

Figure 39. θ **ranges from 0° to 10° with** ϕ **set to 0°.**

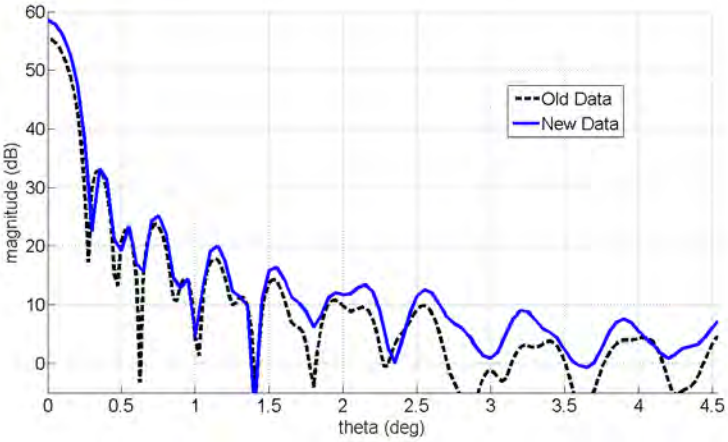

Figure 40. **θ ranges from 0° to 10° with ϕ set to 40°.**

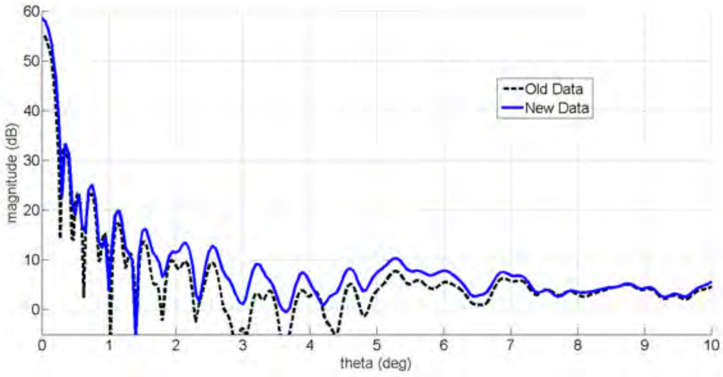

Figure 41. **θ ranges from 0° to 10° with ϕ set to 90°.**

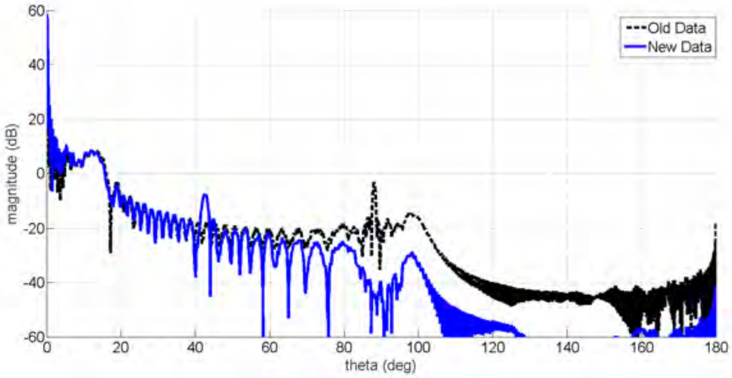

Figure 42. **θ ranges from 0° to 180° with ϕ set to 90°.**

the lobes caused by the struts.

Comparison of the two color maps shows highlights the areas of disagreement.

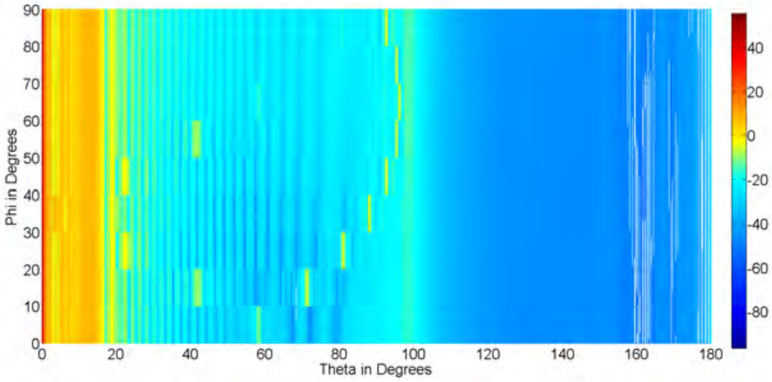

Figure 43. **Color map showing the beam pattern formed from old 10 m data set.**

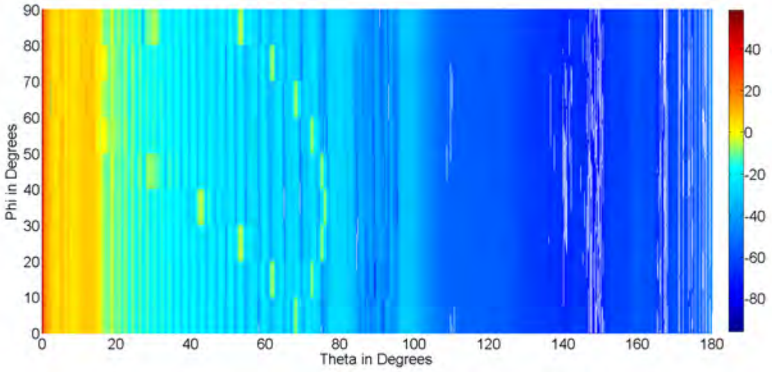

Figure 44. **Color map showing the beam pattern formed from new 10 m data set.**

The previous data set shows strut lobes in areas not predicted by the new data set, and a much higher level in the back lobes. Without having more information about the previous simulations settings, the root cause of these differences can not be determined. Both color maps show a need for a much higher resolution in ϕ for that plot method to be effective.

As a way of showing the difference in results of simulation runs with struts vs without struts, the 10m antenna was modeled without struts in SATCOM. Results from the two new models, with and without struts, were compared against each other. In the new 10 m model without struts, the edge taper was reverted back to the assumed value of -10 dB. Table 10 shows the parameter values used for each simulation. These results show that even with a slight deviation in edge taper and the inclusion of strut effects, the data will still align fairly well. These results confirm that the difference between the old simulations and the new simulations were more than just a deviation in strut angle and edge taper.

For the sake of this research it can be said that the data results for the new simulations of the 10 m cassegrain do not agree with the previous results. The direct cause cannot be attributed solely to a change in edge taper or even a change in strut angle. However, this does not invalidate the results of the current work. The previous work was done in 2016, and the specifics of the simulation's settings were not provided in sufficient detail to enable another person to reproduce them without guesswork.

In an effort to validate the data collected from SATCOM, the SATCOM results for

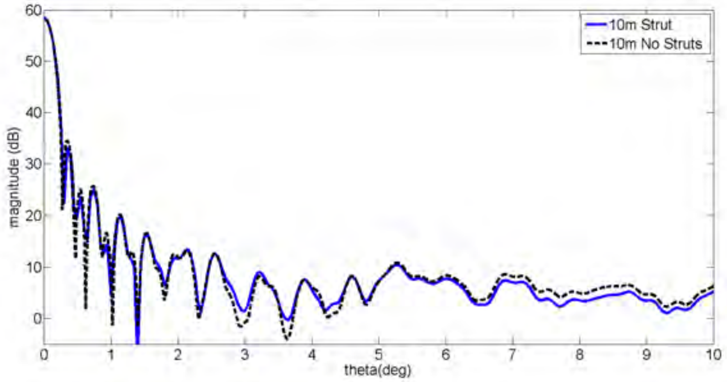

Figure 45. New 10 m SATCOM data struts vs no struts θ 0° to 10° ϕ 0°.

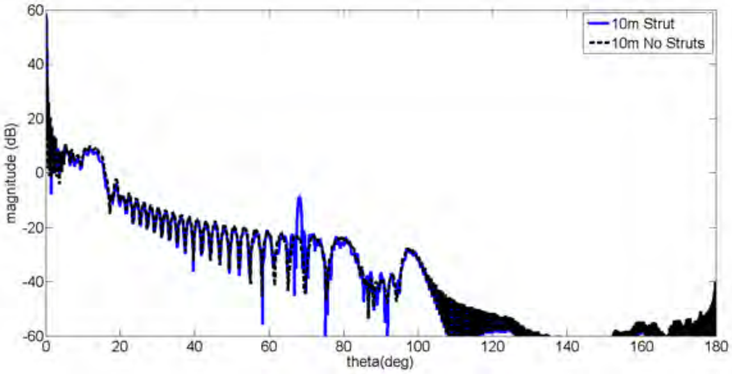

Figure 46. New 10 m SATCOM data struts vs no struts θ 0 to 180 ϕ 0°.

Table 10. Table of parameters used for comparing the results of including struts to not including struts.

Parameter	**Struts**	**No Struts**
Frequency	10 GHz	10 GHz
Polarization	Right Hand Circular	Right Hand Circular
Feed Location	Main Reflector Base	Main Reflector Base
Edge Taper	-11.52 dB	-10 dB
Dm	10 m	10 m
$\frac{F}{Dm}$	0.3125	0.3125
$\frac{Ds}{Dm}$	0.1	0.1
SR Vertex	2.7915m	2.7915m
Eccentricity	1.2712	1.2712
Strut Angle	38°	None

Table 11. Simulation results comparing the new 10 m SATCOM models with and without struts.

	10 m w/ Struts	10 m w/o Struts
Main Lobe Max	58.51	58.52
Half Power Beam Width	0.2°	0.2°
First Side Lobe Max	33.21 dB	34.61 dB
First Side Lobe Location	$0.35°\theta$	$0.35°\theta$

the 10 m data is compared against the results from GRASP. GRASP student edition does not allow for the inclusion of struts in the simulations. The new SATCOM model of the 10 m antenna was adjusted to remove the struts, and the results were compared.

The parameters used for both simulations were as shown in Table 5. Figure 47 displays the results for this comparison. Based on the main lobe and first side lobe values, the two simulations were in agreement. These results are shown in Table 12. Figure 47 displays the two results plotted against each other for a θ range of 0° to 10°.

The two results agree until angles of θ between 1° and 11° θ, refer to Figure 48. The deviation between the two is hard to quantify as the peaks and nulls do not appear to align. At around 11° of θ the two data sets realign and stay relatively aligned until around 80° of θ refer to Figure 49. From 80° of θ on, the two simulations diverge refer to Figure 50. These results are anticipated since the simulations in SATCOM did not include diffraction terms, but results from GRASP include diffraction.

Table 12. Simulation results comparing the new 10 m SATCOM model to GRASP.

	SATCOM	GRASP
Main Lobe Max	58.52	58.45
Half Power Beam Width	0.2°	0.2°
First Side Lobe Max	34.61 dB	34.5 dB
First Side Lobe Location	0.35°θ	0.35°θ

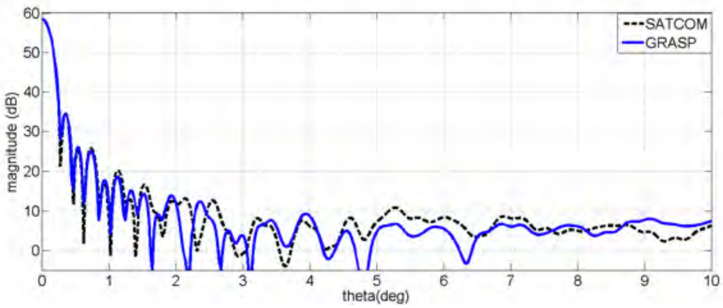

Figure 47. New 10 m SATCOM compared to GRASP 0° to 10°.

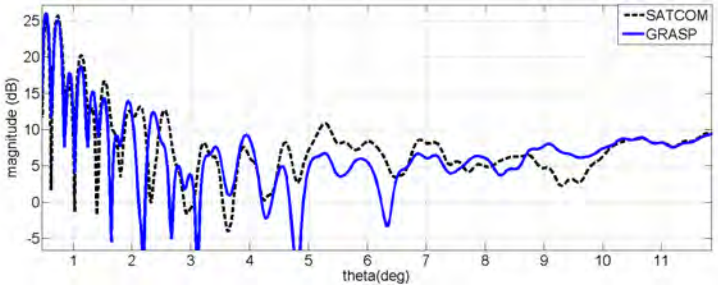

Figure 48. New 10 m SATCOM compared to GRASP 1° to 11°.

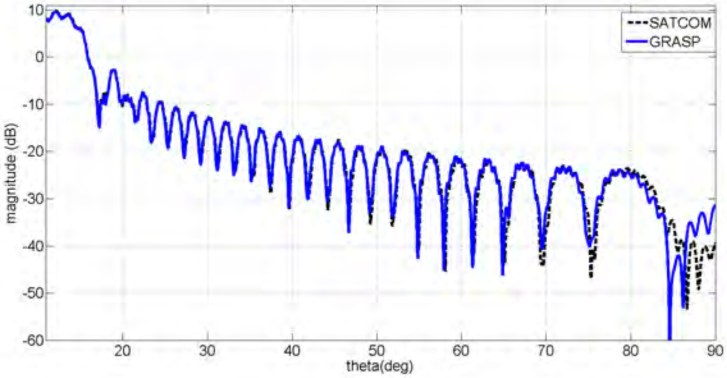

Figure 49. New 10 m SATCOM compared to GRASP 11° to 80°.

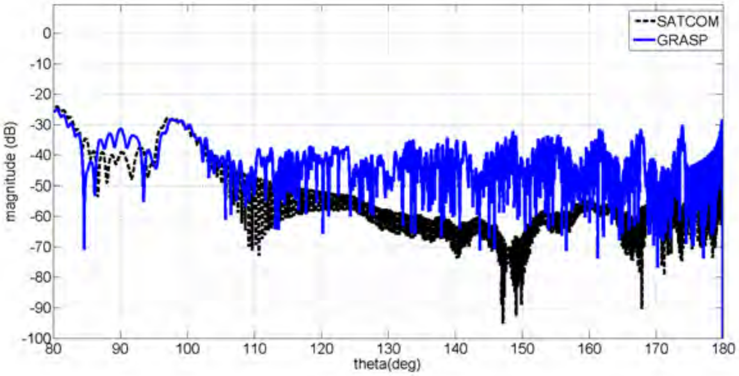

Figure 50. New 10 m SATCOM compared to GRASP 80° to 180°.

4.4 6 m diameter results

As with the 10 m antenna, the 6 m antenna was modeled in GRASP and SATCOM using as close to the same parameters as possible. All of the parameters were scaled as appropriate to keep the same ratios as the 10 m antenna. Simulations in SATCOM were completed for the baseline parameters with and without struts. To build the baseline model with struts, the strut angle was set to the assumed value of 39.26°. Table 13 lists the values used for the assumed configuration, with and without struts.

GRASP and SATCOM results can be compared against each other to help highlight how the inclusion of diffraction impacts the results. Figure 51 shows both simulations plotted against each other. In these models struts were not included.

As with the 10 m case, the inclusion of diffraction terms caused the two simulation results to deviate from one another. In this case the difference started at the first side lobe. The GRASP results showed the first side lobe to be 2dB higher than the SATCOM results. The two simulations began to realign at 8.5° θ. They maintained similar peaks and nulls with GRASP showing values of around 1 dB higher from 8.5° until 20°. Between 20° and 80° the two followed each other very closely.

Table 13. Parameters for the Assumed 6 m antenna with and without struts.

Parameter	**Struts**	**No Struts**
Frequency	10 GHz	10 GHz
Polarization	Right Hand Circular	Right Hand Circular
Feed Location	Main Reflector Base	Main Reflector Base
Edge Taper	-10 dB	-10 dB
Dm	6 m	6 m
$\frac{F}{Dm}$	0.3125	0.3125
$\frac{Ds}{Dm}$	0.1	0.1
SR Vertex	1.6749m	1.6749m
Eccentricity	1.2712	1.2712
Strut Angle	39.26°	None

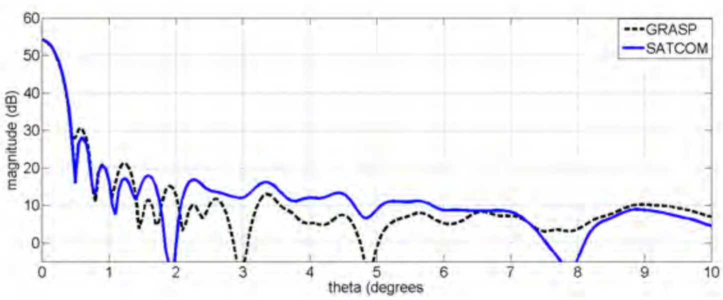

Figure 51. 6 m SATCOM model compared to GRASP.

Table 14. Simulation results comparing the new 6 m SATCOM model to GRASP.

	SATCOM	GRASP
Main Lobe Max	54.15	54
Half Power Beam Width	0.3°	0.3°
First Side Lobe Max	28.16 dB	30.39 dB
First Side Lobe Location	0.6°θ	0.6°θ

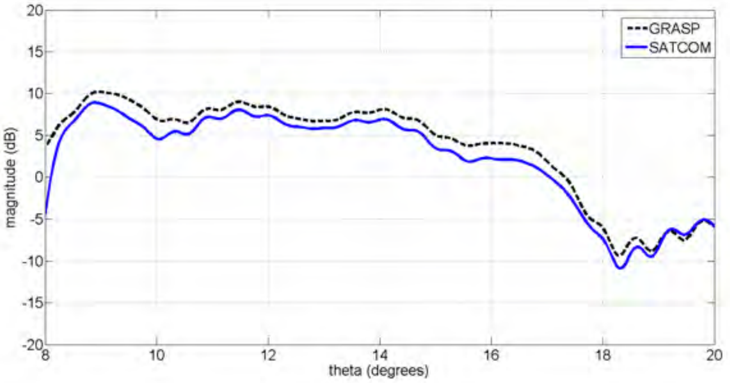

Figure 52. 6 m SATCOM model compared to GRASP from 8° to 20° θ.

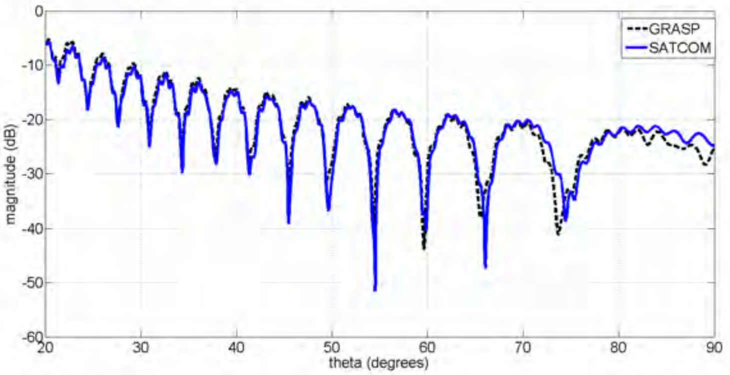

Figure 53. 6 m SATCOM model compared to GRASP from 20° to 90° θ.

After around 80° the two diverged as with the case of the 10 m antenna. Based on the GRASP vs SATCOM results for the 6 m and 10 m antennas the new SATCOM results only include physical optics (PO) effects. The simulation results for this type of model can be accepted for the main lobe level and width. The first side lobe results for the 6 m antenna may or may not be highly accurate depending on geometry. It can be seen from the 6 m and 10 m case that the PO based simulations and the uniform theory of diffraction (UTD) based simulations have fairly decent agreement from the range of about 10° θ until around 80° θ. The magnitude differences were typically within 1 to 2 dB, and the peaks and nulls agreed to within 1°. Based on these results, the sensitivity analysis will include data discussions for the main lobe characteristics and the relative levels of the far side lobe performance.

In order to show the difference between the two plots a little closer, the absolute value of the difference was plotted in dB against the angle θ. Viewing this from 0° to 180° looks bleak for the accuracy of a PO model, but as mentioned there are regions which agree reasonably well, within less than 2dB difference. As an aside the average difference was 3dB, and the peak difference was 35.5dB.

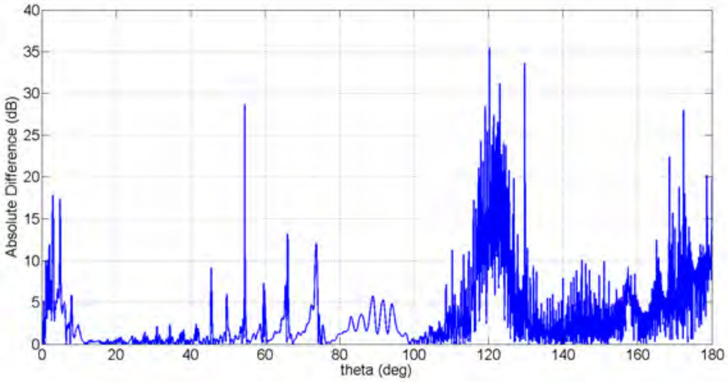

Figure 54. 6 m SATCOM model compared to GRASP from 0° to 180° θ.

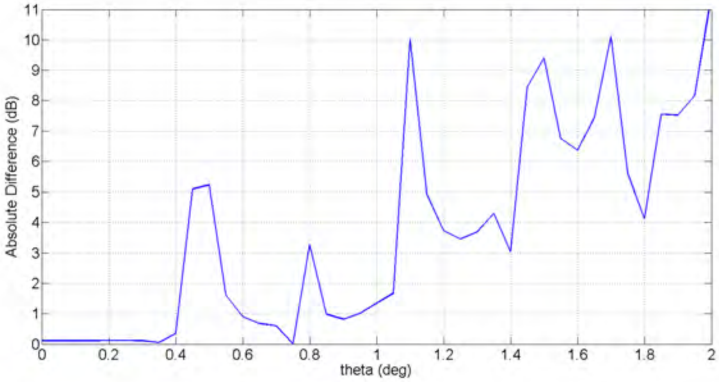

Figure 55. 6 m SATCOM model compared to GRASP from 0° to 2° θ.

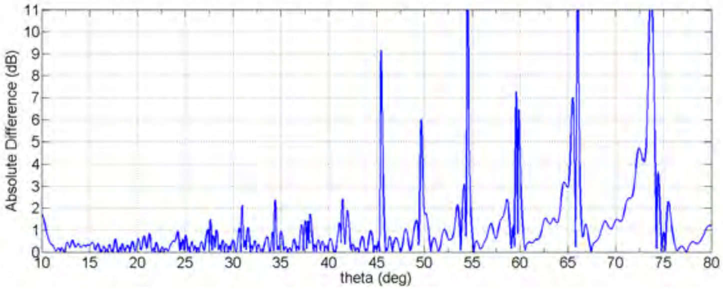

Figure 56. 6 m SATCOM model compared to GRASP from 10° to 80° θ.

There are some difficulties when comparing the two simulation models. The peaks and nulls may not line up directly, and the depth of the nulls ends up impacting the difference plots significantly. Many of the spikes in the difference plots are less than a degree wide, and in some examples they are less than half a degree wide. Figure 57 is plotted with one degree increments in θ and 2.5 dB increments in the absolute difference. Compare this to Figure 58 using the same θ range and θ increment.

Another interesting data point is comparing the results of the simulations which included struts and did not include struts. This allows for supporting the idea that the antenna geometry can be optimized without struts, and then the struts can be added once the optimal geometry is found. As with the 10 m results both simulations will use the assumed configuration as referenced in Table 13. In Figure 59 the plots

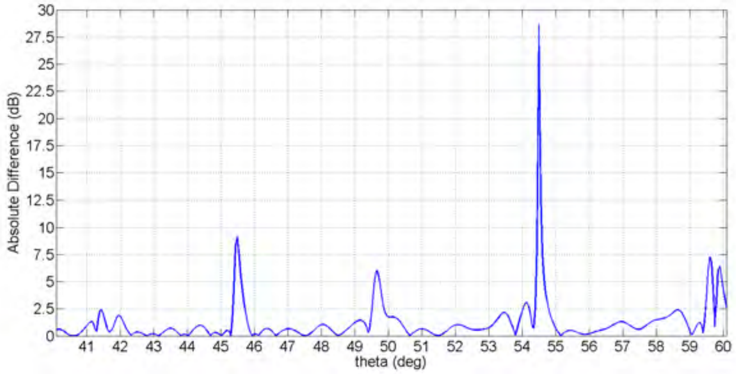

Figure 57. 6 m absolute difference SATCOM model compared to GRASP from 40° to 60° θ.

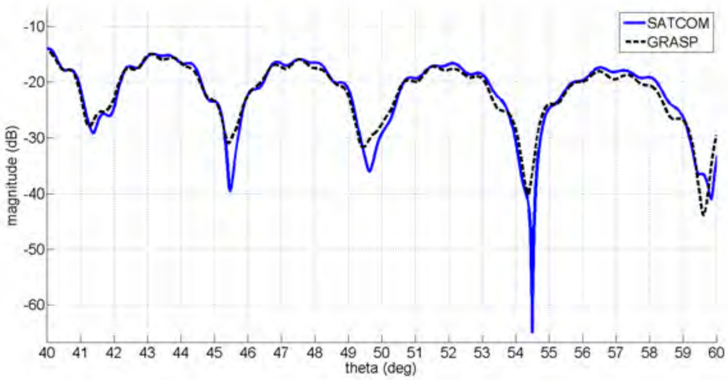

Figure 58. 6 m SATCOM model compared to GRASP from 40° to 60° θ.

are for a ϕ angle of 0° and θ angle 0° to 10°. In this plot it appears as though the two patterns are identical.

Extending the θ plot range out to 180° shows how the two plots compare. There is an obvious difference around 70° which is caused by the struts. Another major difference is that the pattern without struts appears to have a couple points with much deeper nulls.

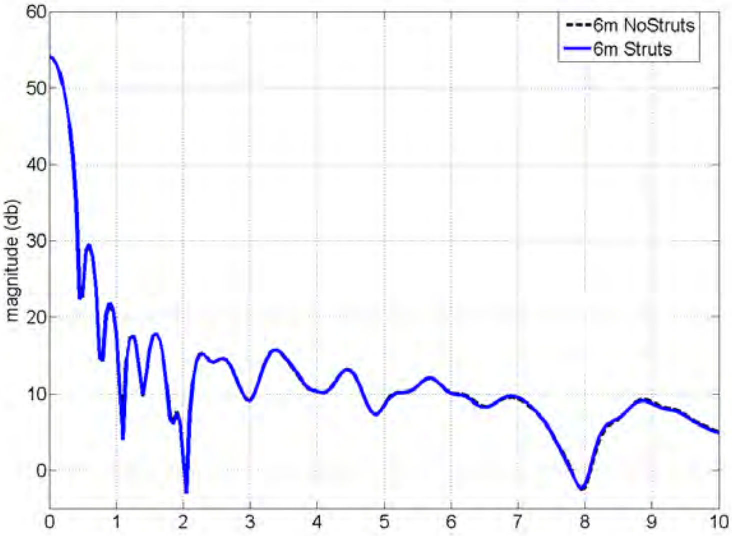

Figure 59. 6 m SATCOM Struts vs No Struts for the assumed configuration 1° to 10° θ 0° ϕ.

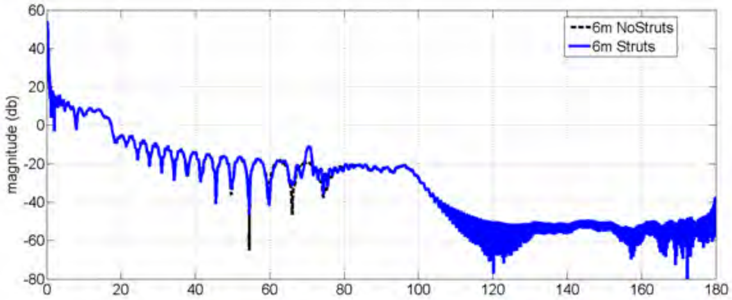

Figure 60. 6 m SATCOM Struts vs No Struts for the assumed configuration 1° to 180° θ 0° ϕ.

Again, a very quick way to visualize the beam pattern simulated is to plot all cuts of ϕ against θ in a color map. This style plot helps highlight the far side lobe effects from the struts. The results for the strut sweep reveal that the conical pattern that begins to appear in the 0° to 90° ϕ range is indeed a repetitive pattern when extended to the -90° to 90° case, see fig. 61.

Looking at other strut angles the conical lobing caused by the struts is dependent on the angle that the struts form with the main axis of the antenna. The more extreme examples from the strut sweep are shown in Figure 62 and Figure 63.

Reviewing the main lobe data from the strut sweeps shows that, as the strut angle is varied, the blockage effects of the struts impact the performance of the antenna. Table 15 demonstrates the effects that the struts have on the main lobe and first side

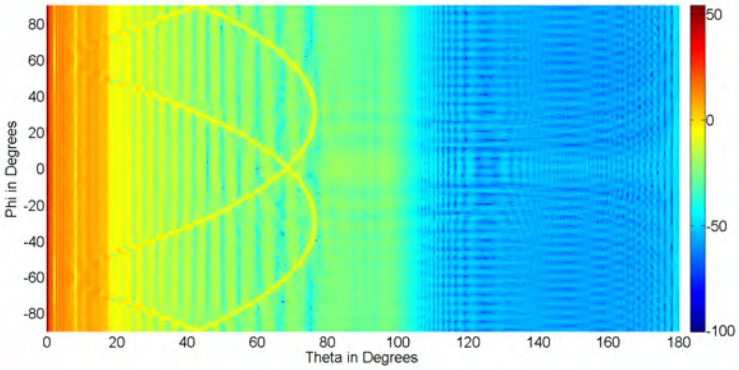

Figure 61. 6 m SATCOM assumed parameters colormap ϕ -90° to 90° θ 0° to 180.

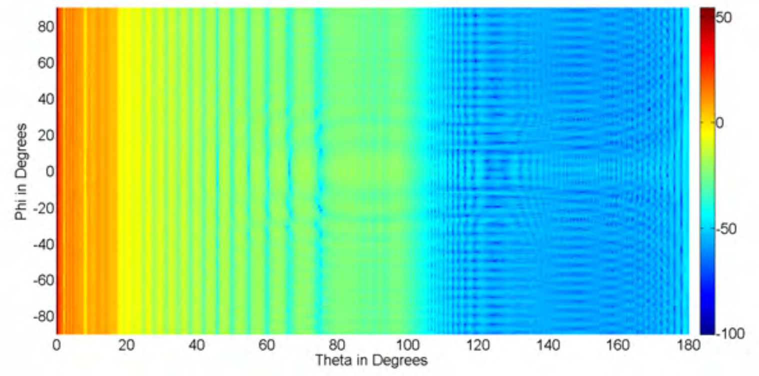

Figure 62. 6 m SATCOM assumed parameters 5° strut colormap ϕ -90° to 90° θ 0° to 180°.

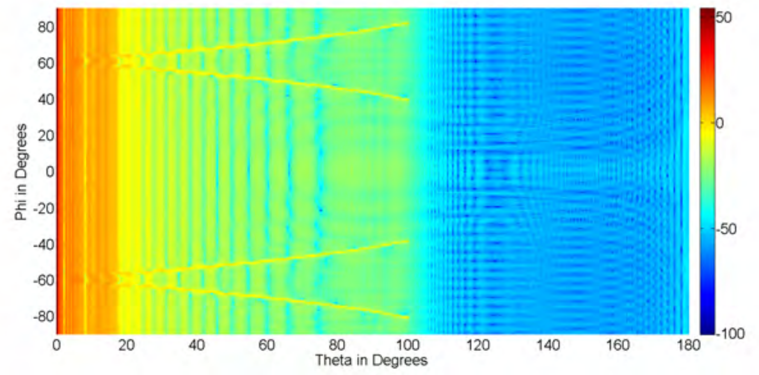

Figure 63. 6 m SATCOM assumed parameters 73° strut colormap ϕ -90° to 90° θ 0° to 180°.

lobe. Evaluation of the effects of changing strut angles was analyzed by performing a strut angle sweep.

Plotting the main lobe maximum value vs strut angle shows that, with the extremely small strut dimensions used, there is less than 1dB change between the minimum strut angle and maximum. The -3 dB beamwidth was not affected. While the strut angle sweep was done with assumed parameters, it is anticipated that this trend would continue for other similar configurations. The take away from this sweep is that the strut angle impacts the main lobe performance and will cause lobe effects which are strut angle dependent.

Parameter sweeps were done for 6 m diameter antenna as a way of performing a

Table 15. **Simulation results comparing the 6 m SATCOM model to GRASP.**

	SATCOM	GRASP
Main Lobe Max	54.15	54
Half Power Beam Width	0.3°	0.3°
First Side Lobe Max	28.16 dB	30.39 dB
First Side Lobe Location	$0.6°\theta$	$0.6°\theta$

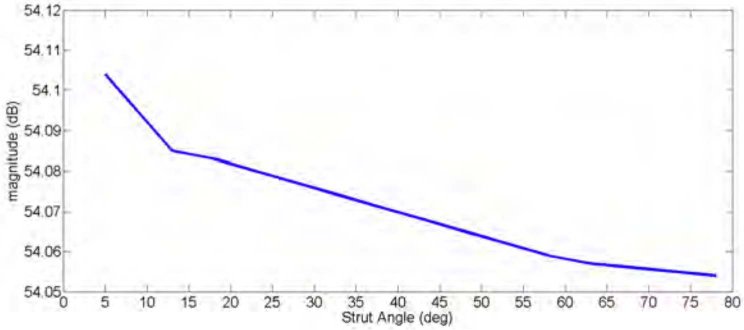

Figure 64. 6 m SATCOM main lobe directivity vs strut angle.

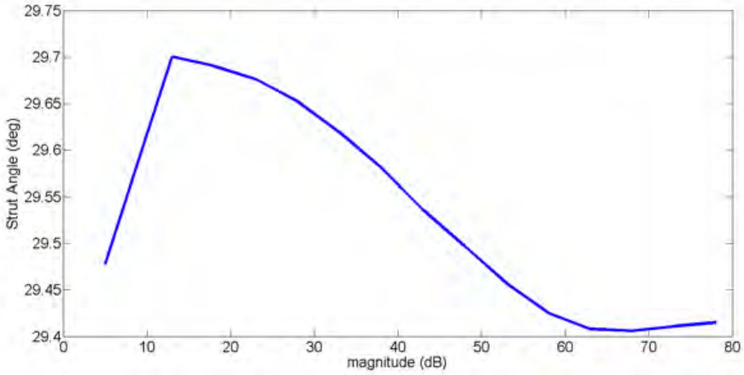

Figure 65. 6 m SATCOM first side lobe level vs strut angle.

sensitivity analysis. During each of these simulations only one parameter was altered at a time while adjusting the other parameters back to the baseline values. Table 16 shows the range and step size for each of these parameters. For all parameters, except $\frac{F}{Dm}$, the range exceeded the typical values used. The value for $\frac{F}{Dm}$ was only extended to 0.6 since values beyond this seemed excessive as compared to the baseline value. At an $\frac{F}{Dm}$ value of 0.6 the focal length of the antenna would exceed 3.6 meters (11.81 feet). The baseline value of 0.3125 converts to a focal length of 1.88 meters (6.17

feet). Each of the increments for the parameters were chosen as an estimated value to allow for smooth plots. In the case of $\frac{F}{Dm}$ and $\frac{Ds}{Dm}$ these incremental values can be converted into a distance measurement. Changing $\frac{F}{Dm}$ or $\frac{Ds}{Dm}$ by 0.01 for a 6 m diameter cassegrain antenna changes the focal length or subreflector diameter by 0.06 m respectively. Incremental changes in eccentricity will incrementally move the the vertex of the subreflector either toward or away from the main reflector. This incremental change is not linear, Figure 66 displays this trend.

As described in the methodology, MATLAB scripts were written to quickly calculate the cassegrain parameters for each of the sweeps. Results from the MATLAB scripts were evaluated and transferred to spreadsheets for ease of reference. De-

Table 16. 6 m parameter sweep range.

	Typical	Sweep Range	Step Size
$\frac{F}{Dm}$	0.1 to 0.8	0.1 to 0.6	0.01
$\frac{Ds}{Dm}$	≤ 0.1	0.01 to 0.3	0.01
Eccentricity	Derived	1.05 to 3.0	0.05
Edge Taper	-15 to -10 dB	-30 to 0 dB	1 dB

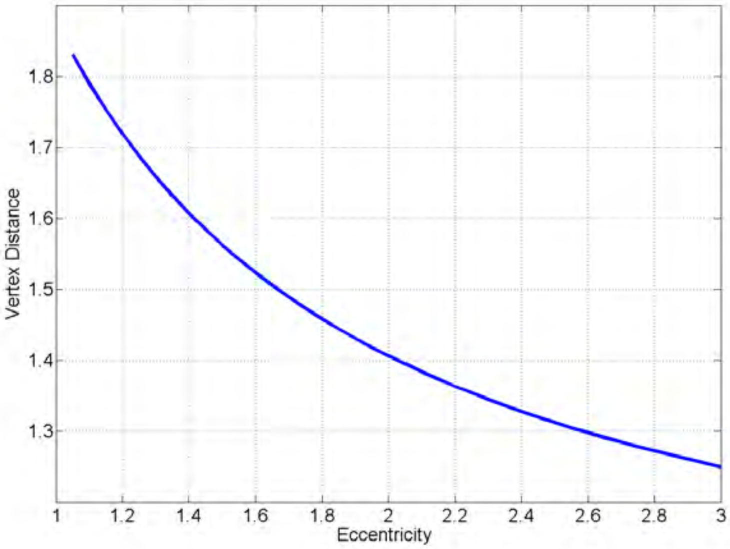

Figure 66. Vertex distance from main reflector for the eccentricity sweep done.

pending on which parameter was varied, one or more of the other parameters were adjusted to maintain consistency with the baseline values. Struts were neglected and symmetries were assumed for each of the parameter sweeps. This leads to each of the simulations only being done for a single value of ϕ and a θ range of 0 to 180. Initial results from the parameter sweeps also pointed toward a need for higher resolution in θ. This need was illustrated by a stair step patterning in various areas of the plots which, ideally, would have been smooth. The higher resolution plots were only done in a range of 0° to 8° θ which far exceeds the range which was identified as usable for this PO only simulation method.

MATLAB scripts were written to read all data files for a parameter sweep, identify the main lobes maximum, the 3dB beam width, and identify the first side lobe level and location. Identifying the first side lobe level and location was done by using the find peaks option to identify the value and index number for the maximum peak. In order to compare the results from the parameter sweeps the assumed configuration values for the main lobe and first side lobe level were used to normalize the corresponding values. This was done to allow an easier understanding of how adjustments impact the performance of the antenna. Equation (28) shows the equation used. The main lobe beamwidth and first side lobe locations were not normalized.

$$NV = AV - PV \tag{28}$$

Where NV is the normalized value, AV is the assumed value, and PV is parameter value. If the adjustment to the parameter results in the same value as assumed the normalized value would be 0.

Reviewing the data for the $\frac{F}{Dm}$ parameter sweep showed that changes in the main reflector's focal length also required changes in the sub reflector's location. Moving the subreflector for alignment purposes resulted in a change in angle between the feed's focal point and the sub reflector's edges. This change would impact edge taper for a given feed design. The MATLAB script for the $\frac{F}{Dm}$ provides correction values to ensure the feed's edge taper is still the assumed -10dB. Table 17 shows a sample of these values.

With the parameters calculated, simulations were done for each of the $\frac{F}{Dm}$ configurations. Results from this were compared against each other with respect to the main lobe maximum level, main lobe beam width, and side lobe level and locations. Figure 67-Figure 70 display the results for the parameter sweep. In these figures the magnitude values are as referenced to the baseline value. Normalizing the data in this fashion allows for a very quick analysis of gain or loss for a specific change in this parameter. The beam width values and location angles are not normalized in this fashion.

Based on the results from the $\frac{F}{Dm}$ sweeps it can be seen that there is some room for improvement in the main lobe performance over the assumed values. The data indicates that, for a given change, the main lobe directivity will only improve slightly. The PO model also indicates that the levels of the back lobes will increase as $\frac{F}{Dm}$ increases. The results for the first side lobe appear to be inconsistent with wild fluctuations, but does show a generally increasing trend. The location of this first side lobe is fairly consistent. Reviewing fig. 71 for the far side lobes using reasonable values, there is not a discernible correlation between lobe levels and $\frac{F}{Dm}$. However, the peaks and nulls in the far side lobes do not appear to shift as a result of the

Table 17. Sample table for $\frac{F}{Dm}$.

F/D	0.28	0.29	0.30	0.31	0.32	0.33
F-Focal Length MR	1.68	1.74	1.80	1.86	1.92	1.98
FC2	1.68	1.74	1.80	1.86	1.92	1.98
FC-Feed to SR Vertex	1.50	1.55	1.61	1.66	1.72	1.77
Source to SR Edge Angle	10.60	10.29	9.99	9.70	9.43	9.18
Feed Value RHCP	268.70	285.54	302.97	320.97	339.55	358.72

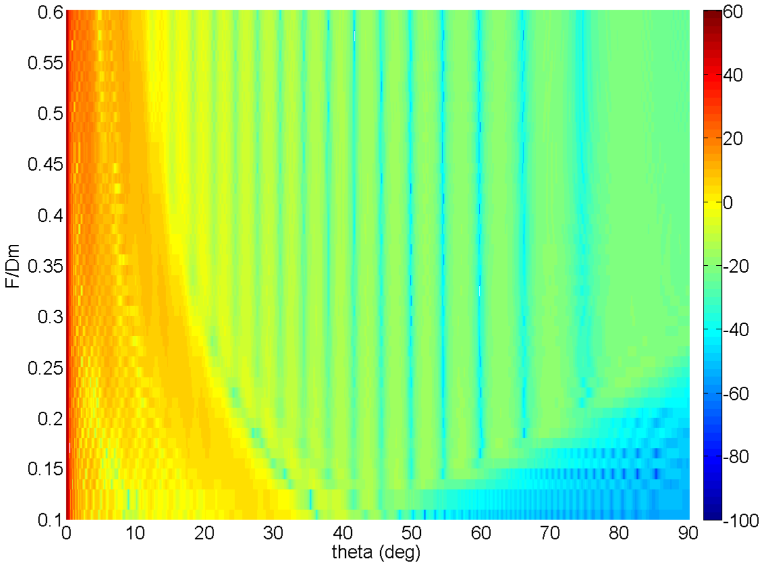

Figure 67. Colormap for the $\frac{F}{Dm}$ sweep.

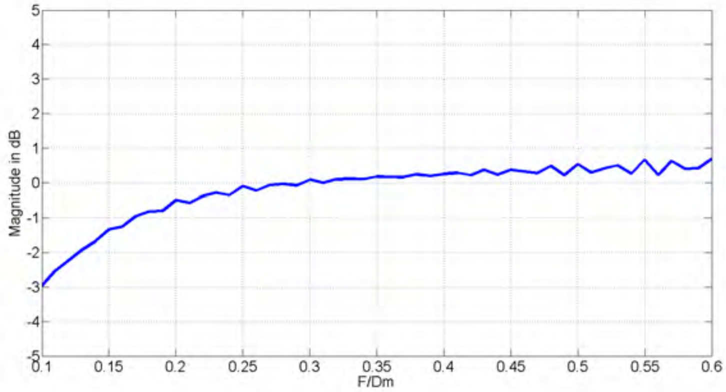

Figure 68. Maximum directivity for $\frac{F}{Dm}$ sweep.

parameter change.

Following the methodology and simulation techniques the remaining parameter sweeps were completed. Table 18-Table 20 show samples for $\frac{Ds}{Dm}$, eccentricity, and edge taper parameters. Figure 72-Figure 85 show plots of the results for the parameter sweeps.

Results from the $\frac{Ds}{Dm}$ sweep appear to indicate that a significantly smaller subreflector would provide a major boost to the directivity of the antenna. The problem

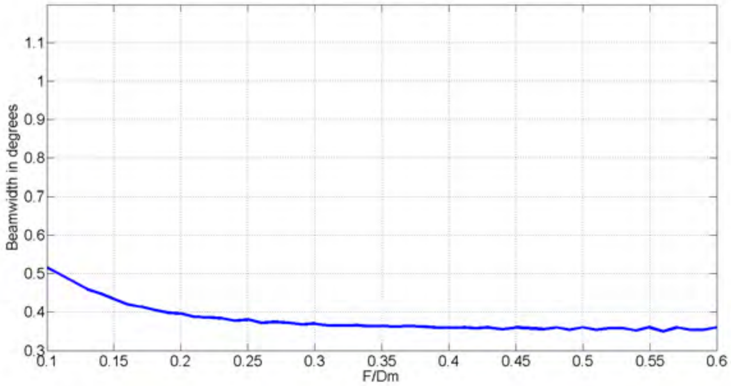

Figure 69. 3 dB beamwidth for $\frac{F}{Dm}$ sweep.

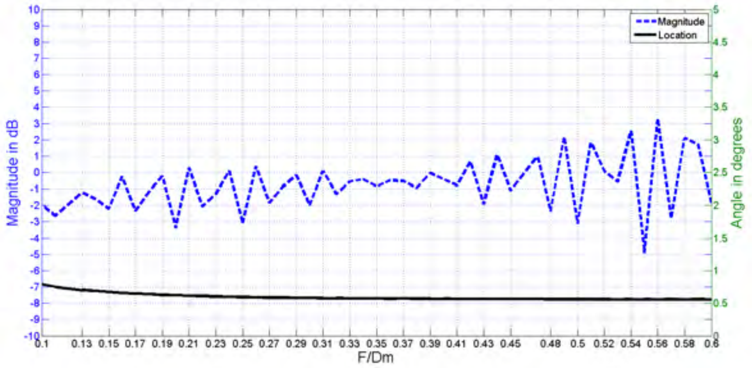

Figure 70. First Side lobe for $\frac{F}{Dm}$ sweep.

with these results is that it is currently infeasible to design the feed to meet the -10dB assumed edge taper. Even at a $\frac{Ds}{Dm}$ of 0.03, the 3dB beamwidth for this feed would need to be less than 3.2°. Looking in the typically accepted values, the results become reasonable. These results indicate that there is room to gain about 1dB of directivity by changing the $\frac{Ds}{Dm}$ from 0.1 to 0.13. This change would also slightly decrease the half power beamwidth, but increase the first side lobe level. Plotting a

Table 18. Sample table for $\frac{Ds}{Dm}$.

Ds/D	0.08	0.09	0.1	0.11	0.12	0.13
Ds	0.48	0.54	0.60	0.66	0.72	0.78
Source to SR Edge Angle	7.87	8.77	9.63	10.47	11.28	12.06
Feed Value for RHCP	487.48	393.10	325.52	275.46	237.32	207.58

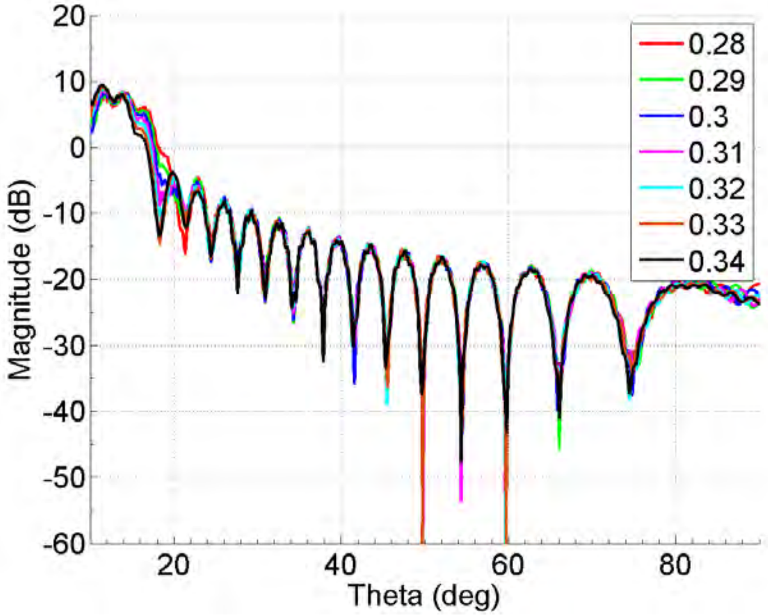

Figure 71. $\frac{F}{Dm}$ **sweep typical values** θ **10° to 90°.**

Table 19. Sample table for eccentricity.

Eccentricity	1.1	1.15	1.2	1.25	1.3
FC-Source to Vertex	1.79	1.75	1.72	1.69	1.66
Source to SR Edge Angle	8.48	8.93	9.26	9.53	9.76
Feed Value for RHCP	419.72	378.39	352.08	332.55	316.86

reasonable range of the sweep values in the range 10° to 90° shows that changes to the sub reflector diameter shift the locations of the peaks and nulls in the far side lobe, see Figure 76.

Results from the eccentricity sweep appear to only show a small region of usable values with 1.2 being the peak value for the assumed parameters. Adjusting to this value of eccentricity appears that it should reduce the main lobe beamwidth slightly, but will increase the first side lobe level. Overall this parameter sweep appeared to

Table 20. Sample table for edge taper sweep.

Taper Value	-15	-14	-13	-12	-11	-10	-9
Feed Value for RHCP	488.34	455.78	423.23	390.67	358.12	325.56	293.00

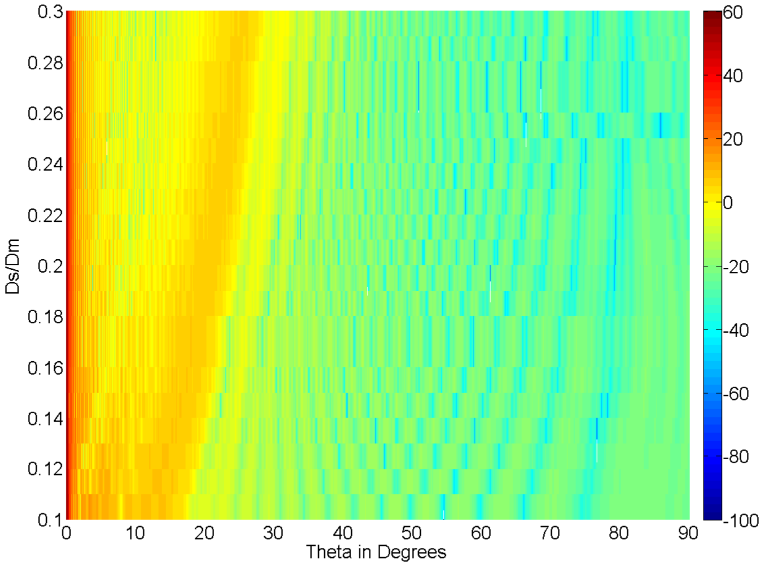

Figure 72. Colormap for the $\frac{Ds}{Dm}$ sweep.

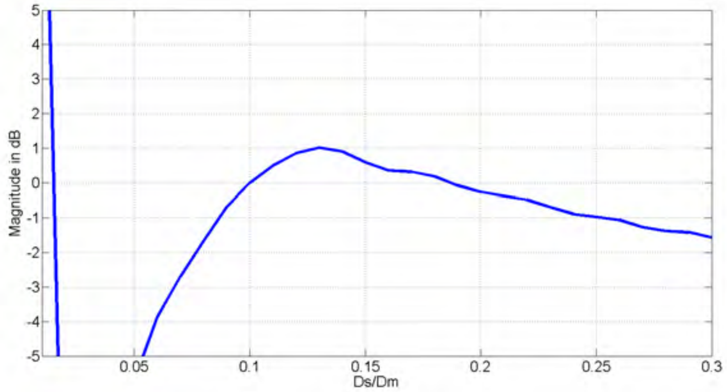

Figure 73. Maximum directivity for $\frac{Ds}{Dm}$ sweep.

indicate that the antenna was more significantly impacted by this parameter than any other. This is likely why the background papers indicated that eccentricity was usually optimized based on the characteristics of the feed and the subreflector diameter. Figure 81 illustrates that in a reasonable range of values the peaks and nulls in the far side lobes do not significantly shift as a result of a parameter change. The peak values do change slightly, and the range of 1.2 to 1.3 appears to minimize the peaks.

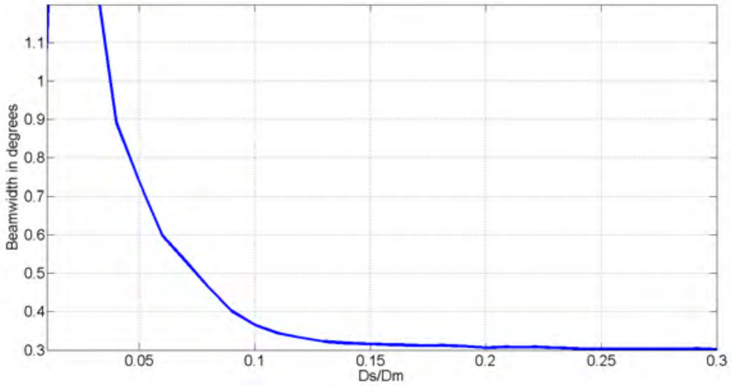

Figure 74. 3 dB beamwidth for $\frac{Ds}{Dm}$ sweep.

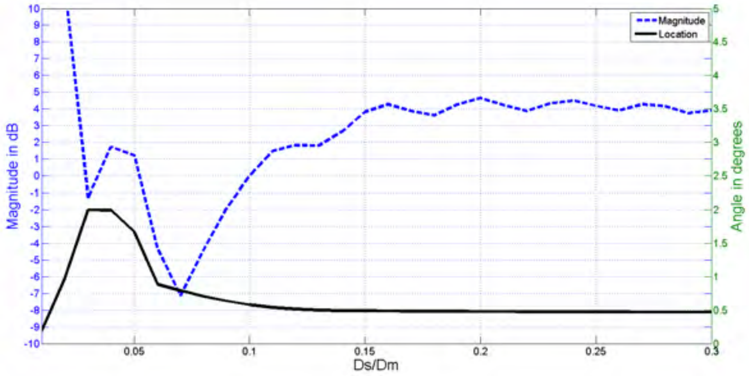

Figure 75. First side lobe for $\frac{Ds}{Dm}$ sweep.

Sweeping the edge taper values showed that an assumed value of -10dB was nearly optimal. Looking at only the main lobe directivity -11dB provides for a gain of less than 1 dB. The typical range of values for edge taper varied by less than 1 dB at the extremes. As with the main and sub reflector sweeps, the eccentricity sweeps were plotted against each other. Figure 86 appears to show that as edge taper is adjusted, in the typical range, that the peaks and nulls remain in the same location. Plotting the parameter also shows that as the edge taper moves from -10 dB to -15 dB the relative far side lobe levels are reduced.

Using the results from the parameter sweeps, it can be seen that the assumed values for the parameters are nearly optimal with regard to directivity and main lobe

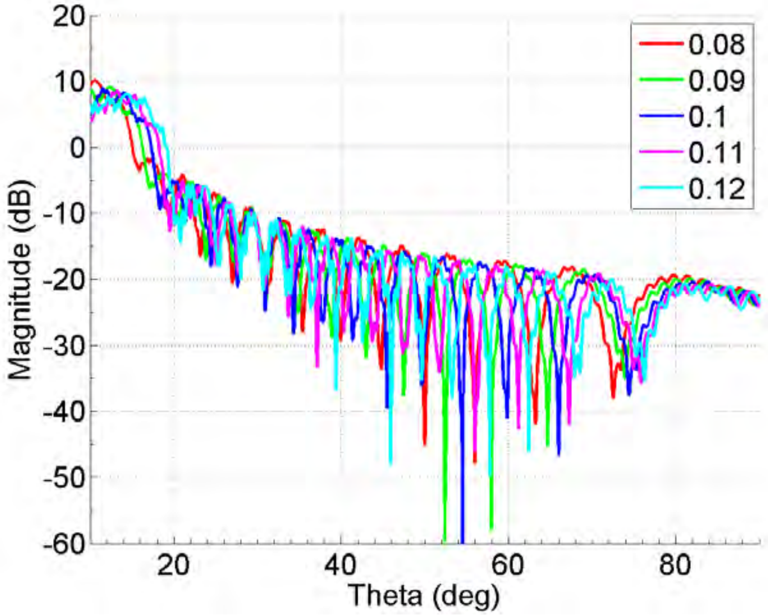

Figure 76. $\frac{Ds}{Dm}$ **sweep typical values** θ **10° to 90°.**

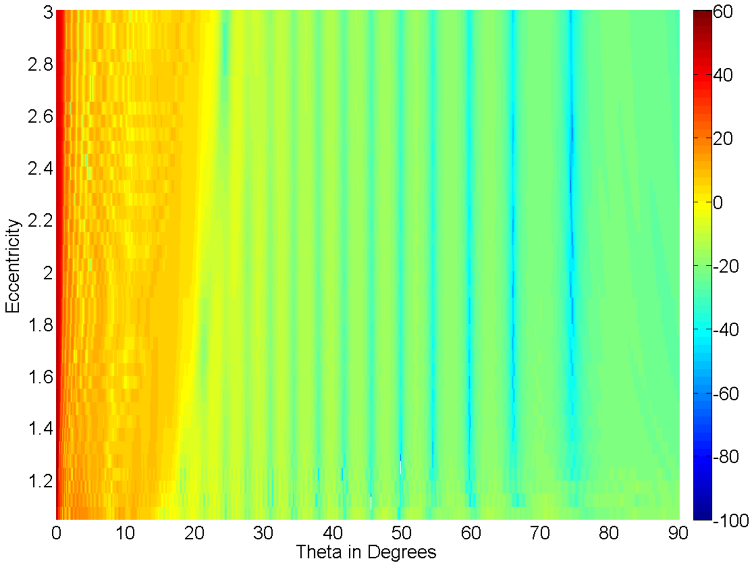

Figure 77. Colormap for the eccentricity sweep.

beam width. While it is tempting to assume that choosing the optimal values for each of the parameters would lead to the optimal design, this is not true. Eccentricity and $\frac{Ds}{Dm}$ adjustments indicated a potential gain of 2 dB for the main lobe directivity.

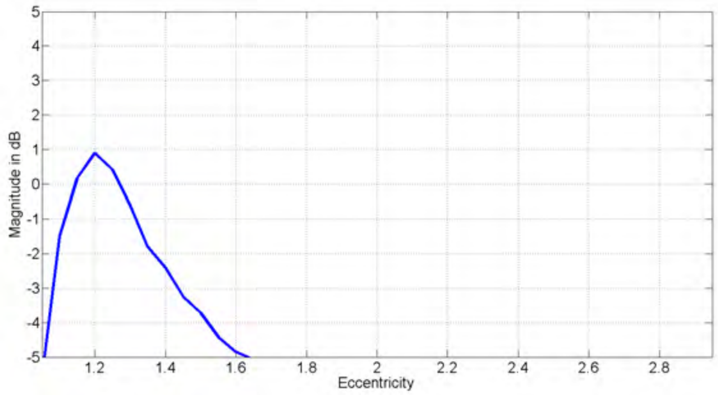

Figure 78. Maximum directivity for eccentricity sweep.

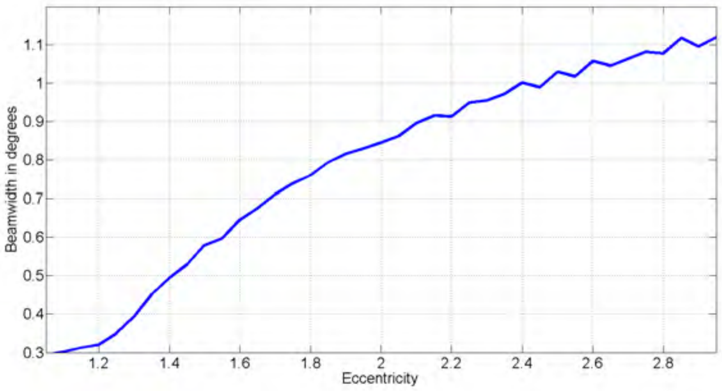

Figure 79. 3 dB beamwidth for eccentricity sweep.

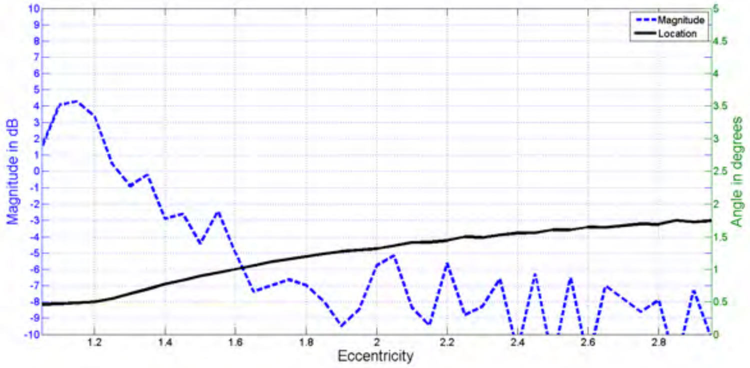

Figure 80. First side lobe for eccentricity sweep.

Increasing $\frac{F}{Dm}$ and changing the edge taper to -11 dB each predicted less than 1 dB of gain. An optimization trial was run using the parameters in Table 21. In this

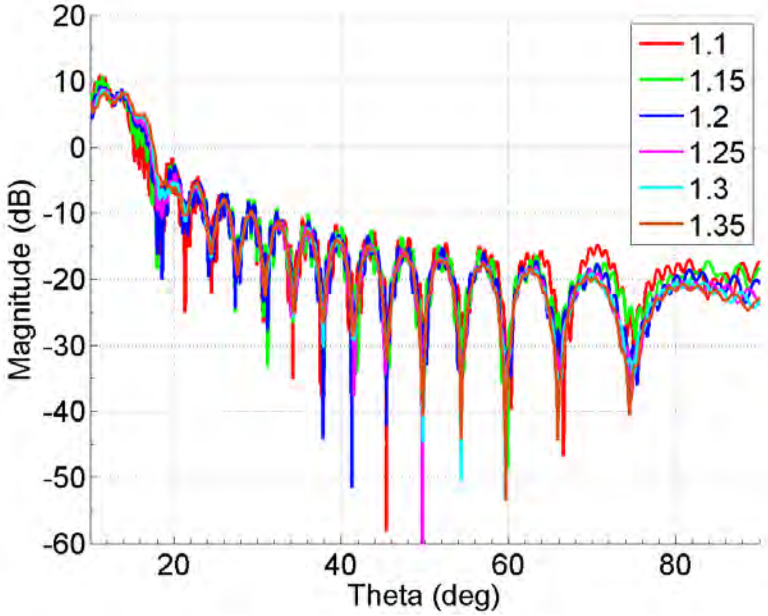

Figure 81. Eccentricity sweep typical values θ 10° to 90°.

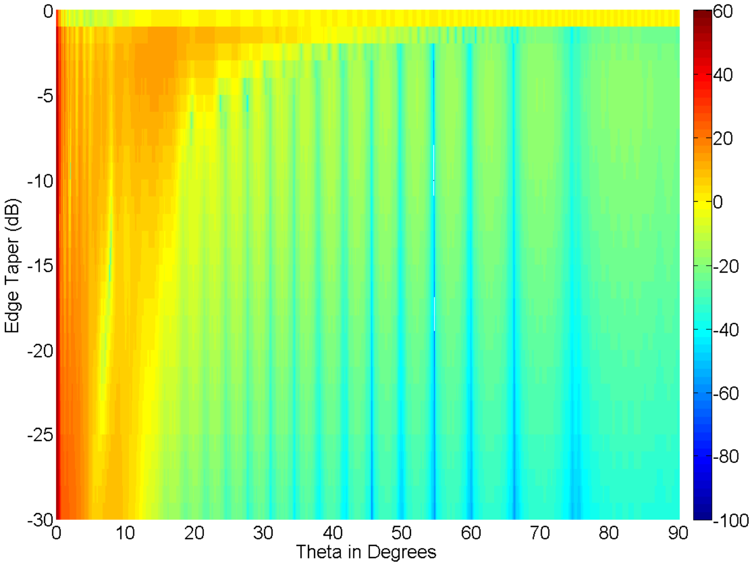

Figure 82. Colormap for the edge taper sweep.

optimization trial, the "optimal" values, with respect to main lobe directivity, for each parameter was used.

The results from this trial show that the antenna acts as a system of components

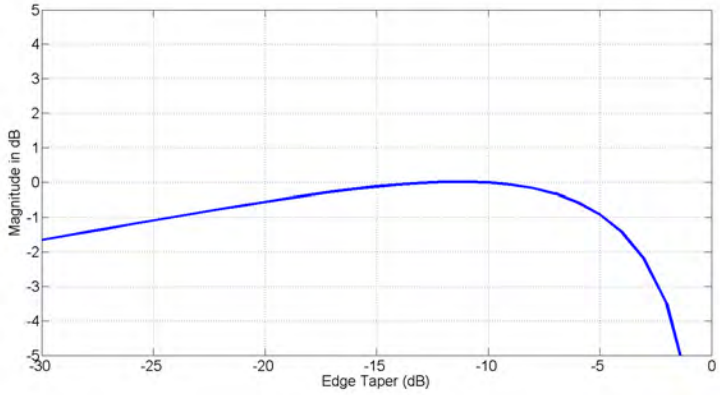

Figure 83. Maximum directivity for edge taper sweep.

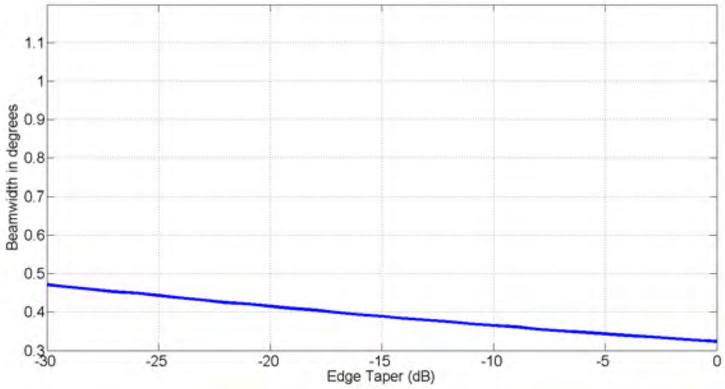

Figure 84. 3 dB beamwidth for edge taper sweep.

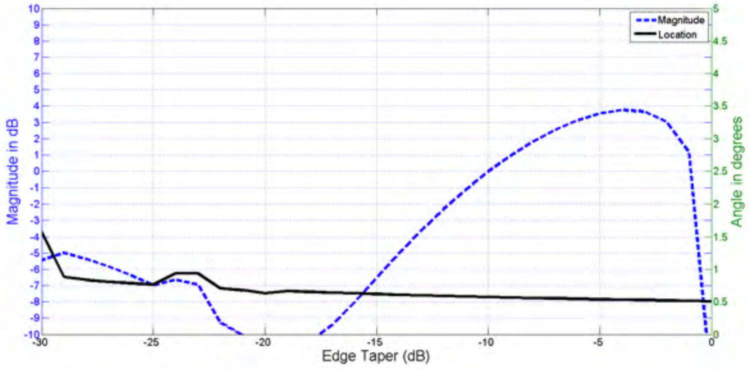

Figure 85. First side lobe for edge taper sweep.

and not individual components. The maximum directivity only increased by 0.5 dB, -3 dB beamwidth stayed roughly the same, and the first side lobe level increased by

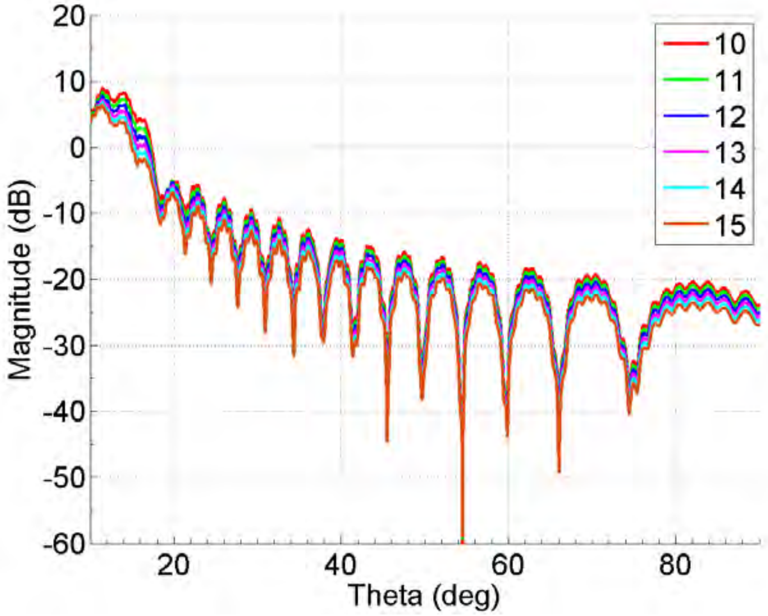

Figure 86. Edge Taper sweep typical values θ 10° to 90°.

3dB. Additionally, the overall beam pattern deviated from the assumed pattern fairly significantly. The average difference between the two in the range of 20° to 80° θ was 5.6 dB. These results led to another optimization trial by setting the eccentricity value and edge taper value, and then sweeping $\frac{Ds}{Dm}$. The results from this trial provided a slight gain on the main lobe directivity and indicated that the optimal $\frac{Ds}{Dm}$ value was 0.1.

Table 21. Parameters for optimization trial.

Parameter	**Assumed**	**Optimization Trial**
Frequency	10 GHz	10 GHz
Polarization	Right Hand Circular	Right Hand Circular
Feed Location	Main Reflector Base	Main Reflector Base
Edge Taper	-10 dB	-11 dB
Dm	6 m	6 m
$\frac{F}{Dm}$	0.3125	0.3125
$\frac{Ds}{Dm}$	0.1	0.13
SR Vertex	1.875m	1.7188m
Eccentricity	1.2712	1.2

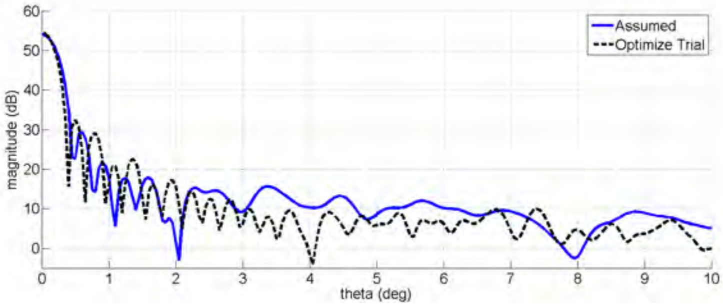

Figure 87. Optimization Trial 0° to 10° θ.

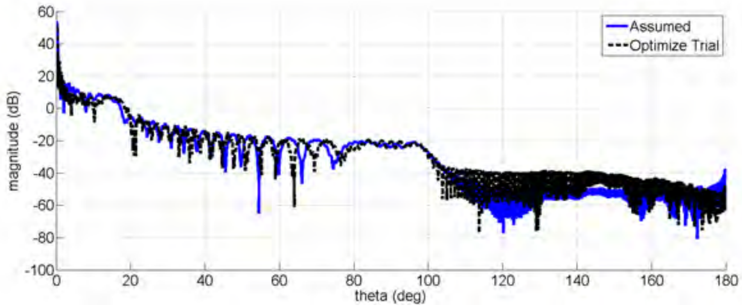

Figure 88. Optimization Trial 0° to 180° θ.

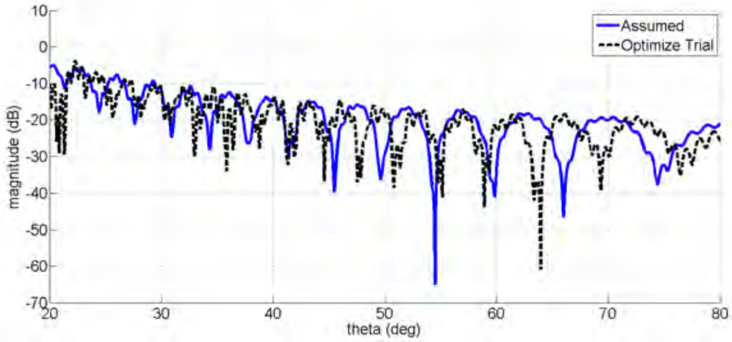

Figure 89. Optimization Trial 20° to 80° θ.

The range of $\frac{Ds}{Dm}$ was limited to between 0.08 $\frac{Ds}{Dm}$ and 0.15 $\frac{Ds}{Dm}$ during the revised optimization trial. The results of these sweeps were compared against each other strictly for main lobe directivity. These results pointed toward 0.1 $\frac{Ds}{Dm}$ being the optimal value for the revised configuration. The results from the sensitivity analysis, trial optimization, and second iteration of $\frac{Ds}{Dm}$ sweeps indicate that an alternative approach to antenna optimization would be needed.

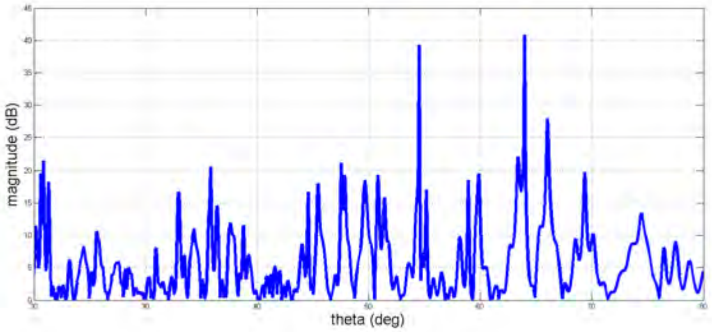

Figure 90. Optimization Trial difference between optimization trial and assumed 20° to 80° θ.

Rather than perform an exhaustive optimization search for this antenna, the revised configuration is shown in Table 22. These values were chosen based on not only the sensitivity analysis, but also the accepted typical design values and the assumptions made during the 10 m characterization work. This configuration will be referred to as "revised" rather than "optimized" or "maximum". This terminology change is strictly to convey that these parameters do not represent an optimal configuration.

Looking at these results without struts lead to a gain of about 1dB on the main lobe and the -3 dB beamwidth stayed unchanged. The first side lobe increased by 3 dB, but the far side lobes remained close to the original level. This is inline with the results from the sensitivity analysis. Moving into the 20° to 80° θ range, the assumed

Table 22. Parameters for optimization trial.

Parameter	**Assumed**	**Revised**
Frequency	10 GHz	10 GHz
Polarization	Right Hand Circular	Right Hand Circular
Feed Location	Main Reflector Base	Main Reflector Base
Edge Taper	-10 dB	-11 dB
Dm	6 m	6 m
$\frac{F}{Dm}$	0.3125	0.3125
$\frac{Ds}{Dm}$	0.1	0.1
SR Vertex	1.875m	1.7188m
Eccentricity	1.2712	1.2

parameters and the revised parameters followed each other fairly closely with respect to the locations of peaks and nulls.

The revised configuration was also simulated in GRASP. As with the assumed configuration, GRASP and SATCOM agreed reasonably well on the main lobe per-

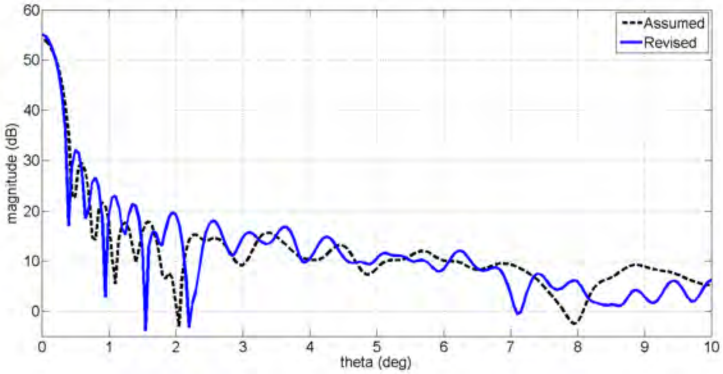

Figure 91. Revised Parameters compared to assumed θ 0° to 10°.

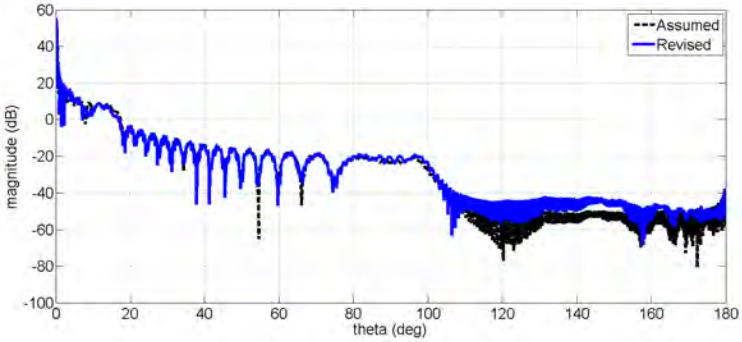

Figure 92. Revised Parameters compared to assumed θ 0° to 180°.

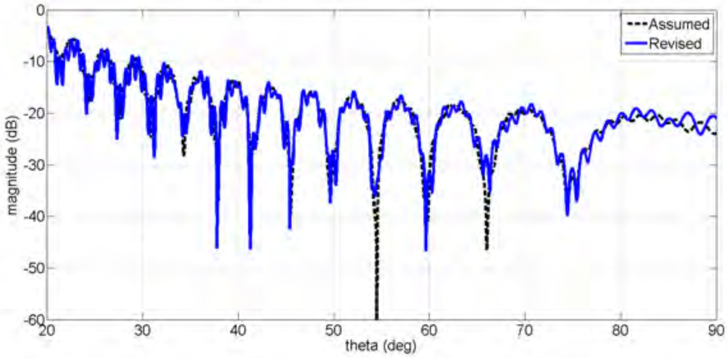

Figure 93. Revised Parameters compared to assumed θ 20° to 90°.

formance as well as the 20 to 80° θ range. The average difference in the 20° to 80° θ region was 2.1 dB.

The parameter sweeps were also repeated for 14 Ghz. These results were reduced to only explore the main lobe and first side lobe. Results from these plots agreed with the results from the 10 Ghz plots. Rather than display repeats for all of the

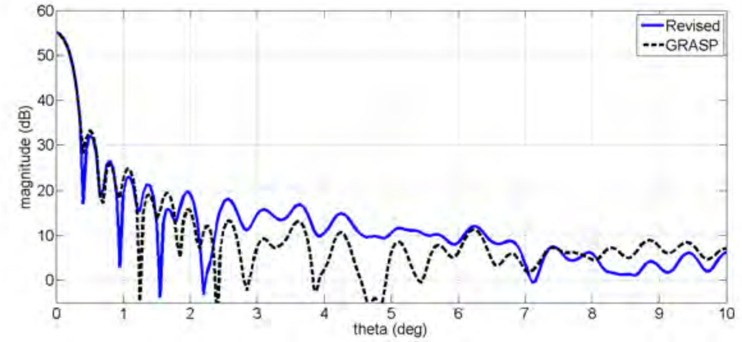

Figure 94. Revised Parameters SATCOM compared to GRASP θ 0° to 10°.

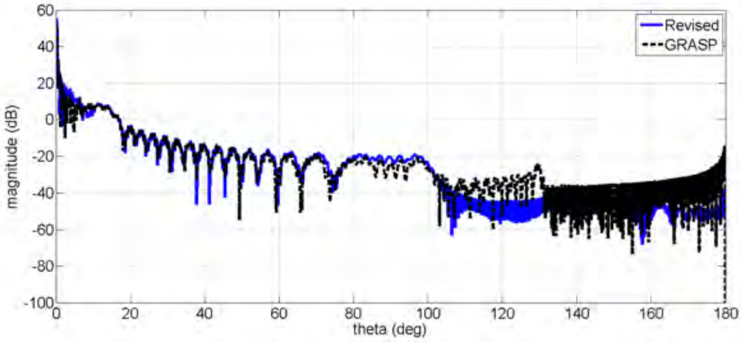

Figure 95. Revised Parameters SATCOM compared to GRASP θ 0° to 180°.

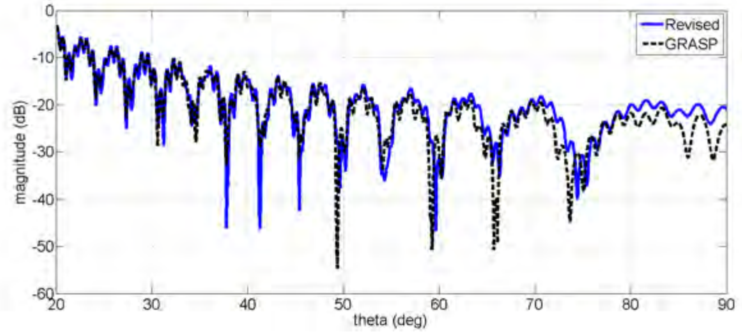

Figure 96. Revised Parameters SATCOM compared to GRASP θ 20° to 90°.

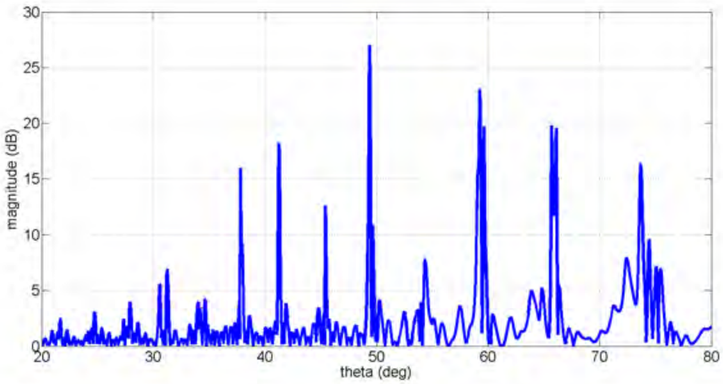

Figure 97. Revised Parameters difference between SATCOM and GRASP results for θ 20° to 90°.

plots, Figure 98-Figure 101 shows just results for how the sweeps changed the main lobe directivity.

Based on the results from the 14 GHz sweeps, parameter changes are anticipated to behave in the same manner as the 10 GHz parameters. Comparing the assumed configuration at both 10 and 14 GHz shows that at 14 GHz the main lobe level is slightly higher and the beam width is a narrower.

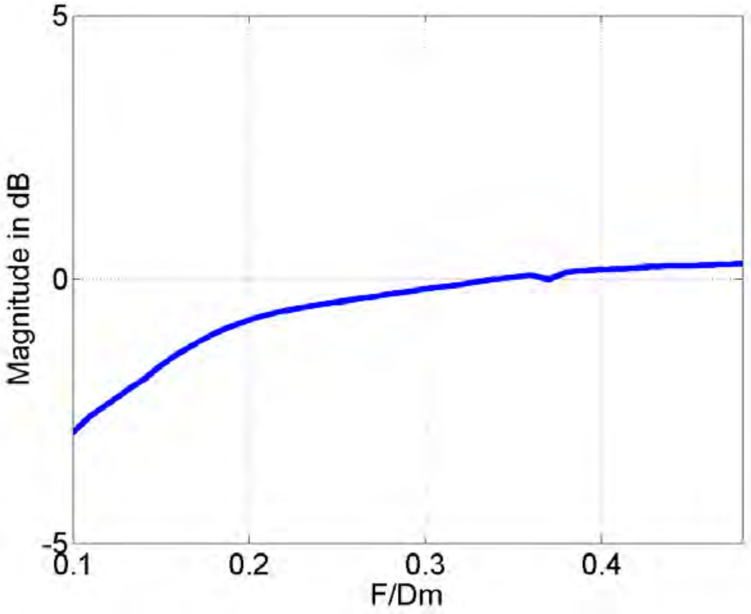

Figure 98. Maximum directivity for $\frac{F}{Dm}$ sweep at 14 GHz.

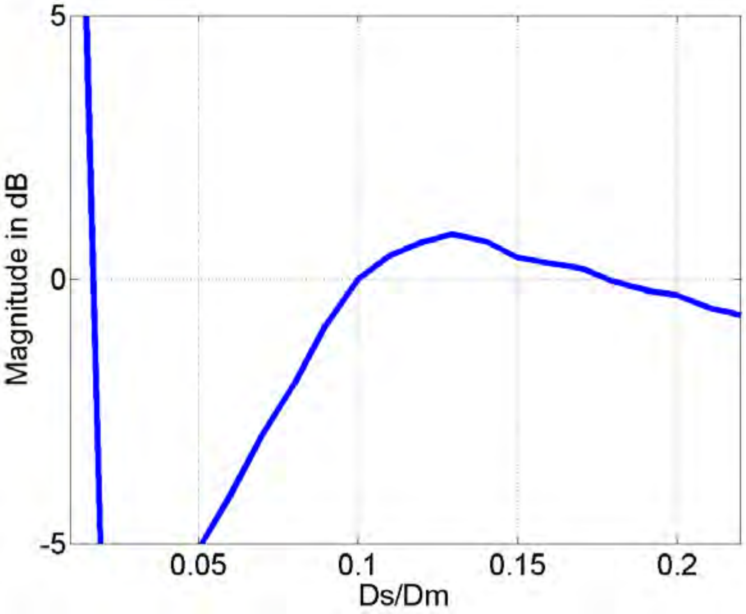

Figure 99. Maximum directivity for $\frac{Ds}{Dm}$ sweep at 14 GHz.

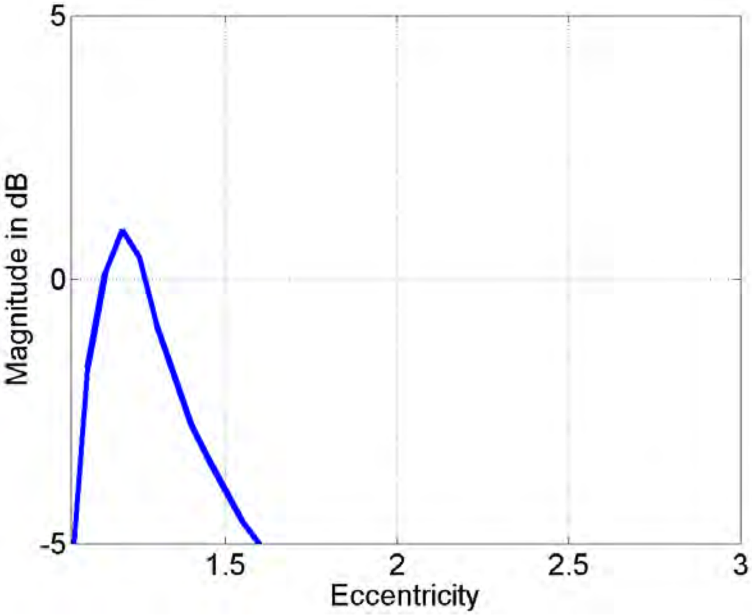

Figure 100. Maximum directivity for eccentricity sweep at 14 GHz.

Reviewing the far side lobe data shows that the far side lobes are of similar levels, but the peaks and nulls are shifted.

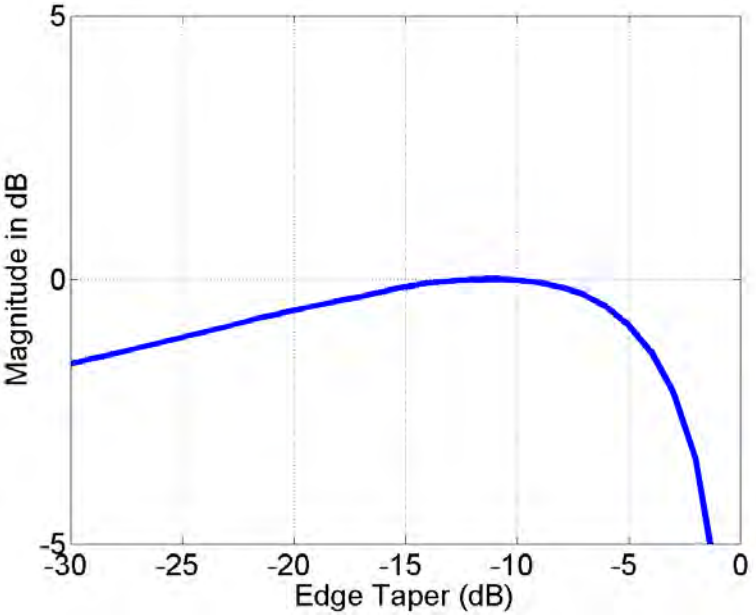

Figure 101. Maximum directivity for edge taper sweep at 14 GHz.

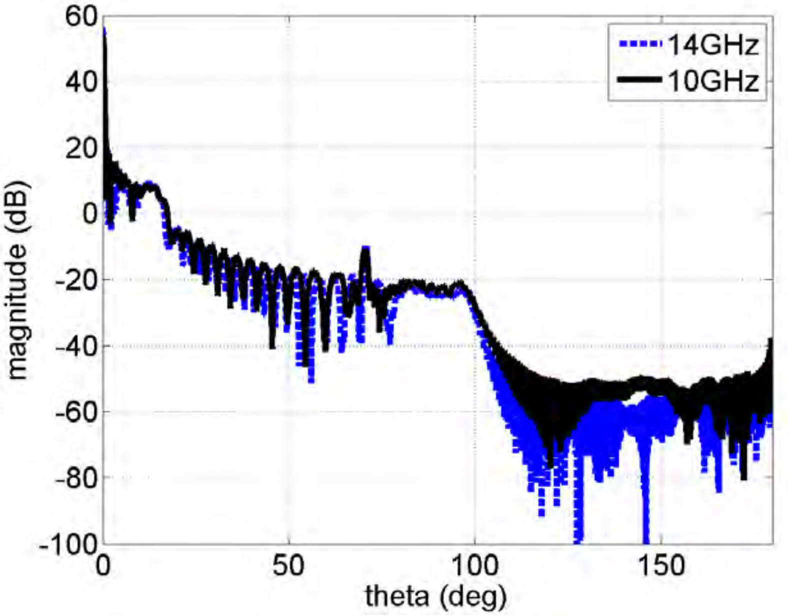

Figure 102. Assumed configuration compared at 10 GHz to 14 GHz at θ 0° to 180° and ϕ 0.

Results from the 14 GHz demonstrate how the antenna will scale as a function of frequency. The 6 m antenna is 200 λ when the design frequency is 10 GHz, and when

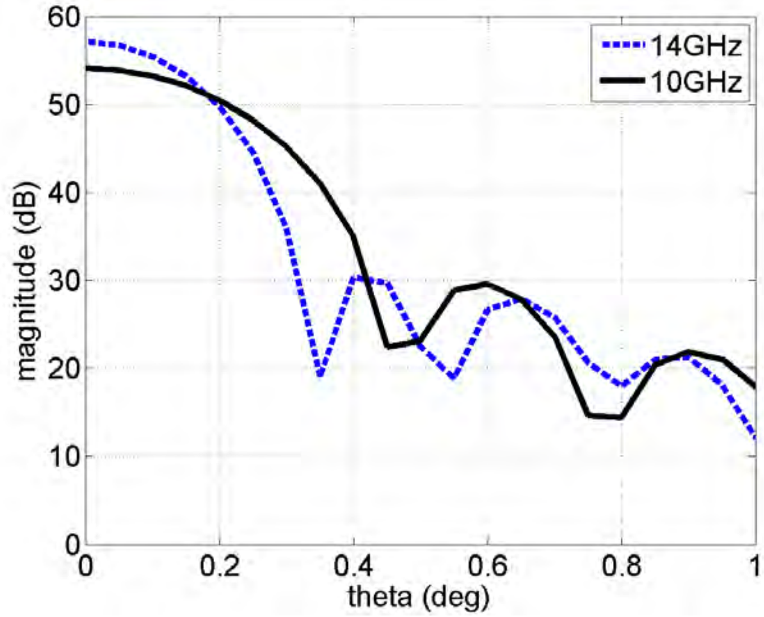

Figure 103. Assumed configuration compared at 10 GHz to 14 GHz at θ 0° to 1° and ϕ 0.

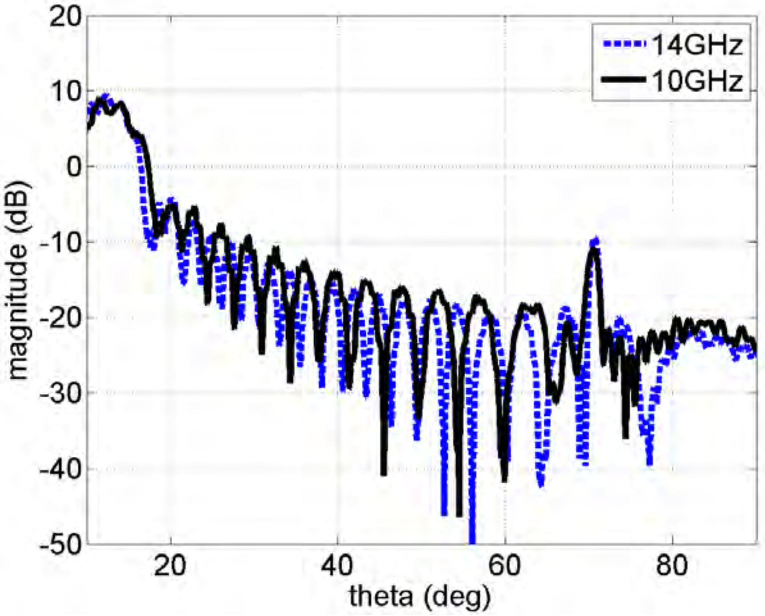

Figure 104. Assumed configuration compared at 10 GHz to 14 GHz at θ 10° to 90° and ϕ 0.

the design frequency is 14 Ghz the 6 m antenna is 280 λ. For comparison purposes the 10 m antenna is 333 λ at 10 GHz and 466 GHz at 14 GHz. Using these points of

Table 23. Simulation results, assumed configuration compared at 10 GHz to 14 GHz.

	10 GHz	14 GHz
Main Lobe Max	54.07	57.12
Half Power Beam Width	0.366°	0.264°
First Side Lobe Max	29.6 dB	30.3 dB
First Side Lobe Location	$0.6°\theta$	$0.4°\theta$

information about scaling it can be seen that the cassegrain antennas peak directivity scales as a function of frequency.

Table 24. Simulation results comparing the main and first side lobe as a function of lambda.

	10 GHz 6 m	14 GHz 6 m	10 GHz 10 m
λ	200	280	333
Main Lobe Max	54.07	57.12	58.51
Half Power Beam Width	0.366°	0.264°	0.2°
First Side Lobe Max	29.6 dB	30.3 dB	33.21 dB
First Side Lobe Location	$0.6°\theta$	$0.4°\theta$	$0.35°\theta$

V. Conclusions

This research focused on characterizing a 6 m diameter Cassegrain antenna through the use of simulations. The approach was to do a sensitivity analysis on the individual parameters based on an assumed configuration. In an effort to validate the simulations, comparisons between GRASP and SATCOM were done. All of these efforts resulted in the presentation of a potential performance band for the 6 m antenna. The general methodology for analyzing the results presented a unique perspective on performance impacts from a single parameter change. Combining the "optimal" values from each of the parameter sweeps does not result in an optimized antenna. If the goal is to optimize the antenna's design, then an alternate approach is necessary. The following sub sections will summarize the conclusions for each of the parameters and the simulation comparison.

5.1 Simulation Comparisons

Evaluating not only the direct comparisons of the simulations, but also the descriptions used in the software suites, it can be concluded that the SATCOM models used in this research did not include uniform theory of diffraction (UTD) effects. GRASP appeared to provide a combined model of physical optics (PO) and UTD effects. SATCOM was the software used predominately in this work. Availability constraints on other software suites drove this decision. Since this software was sourced from Ohio State University (OSU), it is not generally available for others to use.

When comparing the results from GRASP and SATCOM it can be seen that they are within 1 dB of agreement for the main lobe. The main lobe beamwidth is also very similar. Moving further away from the main lobe the diffraction effects start to impact the results, but diffraction effects were minimal in the range of 20° to 80° of

θ.

5.2 Strut Angle Effects

Based on this work, it can be seen that minimizing the strut angle with respect to the main axis of the antenna results in minimizing blockage effects. As the strut angle is increased, the blockage effects become more pronounced. SATCOM modeling predicts peaks in the far side lobes which are caused by the struts. Attempting to identify the strut effects in single cuts of ϕ proved futile. However, representing the 3-D beam pattern data as a color map was a very efficient way of identifying where these side lobe disturbances could be found. Based on this work, the only conclusion which can be made is that struts will likely cause disturbances in the far side lobes. In this work the strut configuration was assumed based on the previous work. Due to the nature of the struts, there is a nearly infinite level of possible adjustment. A more in-depth look at how strut configurations impact the far side lobes should be completed.

5.3 F/Dm Change Effects

Within the bounds of the simulations done, increasing $\frac{F}{Dm}$ showed a continuous increase in main lobe directivity and a decrease in beamwidth. Increasing $\frac{F}{Dm}$ does have the trade off of increasing strut lengths and requiring a narrower feed beamwidth. This is a result of changing the focal length for a given diameter. From an $\frac{F}{Dm}$ of 0.25 to 0.6 there was an average change of less than 1 dB. Its is likely that keeping the $\frac{F}{Dm}$ around 0.3 would be optimal. Using values near 0.3 should reduce the structural requirements to properly locate the sub reflector. Increasing $\frac{F}{Dm}$ would increase the main reflector's surface area and the amount of material required for the reflector's surface.

5.4 Ds/Dm Change Effects

Results from the $\frac{Ds}{Dm}$ sweep were very interesting. While it appears that having an extremely small $\frac{Ds}{Dm}$ would be optimal, the reality is that achieving the -10 dB edge taper for incredibly small sub reflector diameters would be very difficult. Using the configuration as simulated, a $\frac{Ds}{Dm}$ of 0.05 would lead to a 0.3 m diameter sub reflector. The source to edge angle would then be 5° leading to required -3dB beam width of 5.5° to meet the -10dB edge taper, assuming the same feed profile from the simulations. Referencing the simulation values, 0.05 is around 5 dB down from the assumed values. If all of the parameters were as assumed, the peak value which was considered reasonable was 0.13. This leads to a subreflector diameter of 0.78m and a source to edge angle of around 11.28°. Again, using the feed taper profile from the simulations this would lead to a -3dB beamwidth of around 12°, which is feasible for a horn style antenna. Based on the simulation results, a range of 0.1 to around 0.19 $\frac{Ds}{Dm}$ would lead to similar or better results than the assumed configuration. Typically, the diameter of the subreflector is chosen to be less than 0.1 $\frac{Ds}{Dm}$. The simulations as conducted indicate that values less than 0.1 $\frac{Ds}{Dm}$ would cause a reduction in performance compared to the assumed configuration.

5.5 Eccentricity Change Effects

Eccentricity is another parameter which showed potential for increasing the antenna performance over that of the assumed values. The value as assumed was 1.2712, and the ideal value based on the simulations was 1.2. At a value of 1.2 the main lobe maximum value would increase by about 0.9 dB. Values for eccentricity between 1.15 and 1.3 would maintain similar or better performance compared to the assumed configuration. With regard to subreflector vertex positioning, this leads to a range of about 1.75 m to 1.66 m. The peak value of 1.2 led to a vertex positioning of 1.72 m.

The source to subreflector edge angle changes from 8.9° to 9.7°. Changing from the assumed value to 1.2 lead to minimal changes to other parts of the beam pattern. While slight deviations from this value are indicated to have a performance loss, these values would still be equal to or better than the assumed values.

5.6 Edge Taper Change Effects

The assumed value of -10 dB edge taper was very close to the ideal value. Changing this in the assumed configuration to -11 dB led to a slight gain of 0.023 dB. From an edge taper of around -20 dB to around -6 dB, the maximum loss from the assumed configuration is only 0.5 dB. This points toward the assumed configuration being relatively stable across a wide range of edge tapers. The feed's edge taper and the subreflector attributes are strongly linked. Based on the background papers used for this research the ideal situation is to know the feed pattern of the source to be used, and then optimize the subreflector properties to the known feed pattern.

5.7 Future Work

While results from this work have provided insight into the ideal operations of a 6 m cassegrain antenna, there is a lot of room for future work. Researching cassegrain antennas returns work being done in frequency selective surfaces, changes to the feed structure, offset designs, steerable configurations, adjustable beam widths, and much more. The following itemized list provides potential topics of future work which could build directly from the research documented in this paper.

- The lack of UTD effects in the simulations limits the accuracy of the results. Repeating all of the parameter sweeps with UTD effects include will allow for a more accurate analysis of the parameters.

- Perform a power handling study focusing on the differences in subreflector shaping. This power handling study should include the traditional hyperbolic subreflector, parabolic subreflectors, and potentially other shapes. The goal of this study would be to establish which shaping has the highest power handling capability prior to exhibiting breakdown. A secondary goal of this study would be to understand how the far side lobes are affected by changing the sub reflector's shape.

- Change the shape of the reflectors from circular to elliptical and perform a similar sensitivity analysis. When using a circularly polarized feed and circular dishes, the beam pattern is symmetrical with respect to azimuth and elevation. Changing these reflectors to have an elliptical shape should allow for a non symmetrical beam pattern.

- Further analysis is needed on the impacts of struts. In this work the strut configuration was limited to help control the scope of this research. Future work on the strut analysis could start with evaluating the impacts of a single strut at various angles, and then extend this to include multiple struts with various geometries. Ideally the work would result in a well defined relationship which can forecast where the far side lobes would be disturbed without the need of doing extensive simulations.

- Conduct test and measurement on a re-configurable cassegrain antenna to determine the validity of simulation results. Theoretically, by increasing the source frequency the physical size of the antenna can be adjusted proportionally to maintain similar performance characteristics. Physically smaller antennas would enable using a much smaller test facility, but the manufacturing tolerances on the antenna would be significantly tighter than the original size.

Appendix A. MATLAB Scripts

1.1 Sample Parameter Sweep Script

```
clc
clear all
close all
% setting a count variable
count=0;
% Sweeping Ds/D
DSL=0.01:0.01:0.3;
% Dish sizes of interest
DD =[6 10]
for D=DD
count= count+1;   % Book Keeping for the arrays built
countF=0;         % Reseting Counter for next dish ...
    size of interest
for DS=DSL;
countF=countF+1;
% General Calcs
FoD=0.3125;
F(countF,count)=D*FoD;                   % Focal length ...
    calculation
FC(countF,count)=F(countF,count);        % Storing the ...
    various focal lengths
```

```
DsoD=DS;         % Diameter of the sub reflector to ...
    main reflector ratio
Ds=D*DsoD;       % Calculating the sub reflector diameter
%Setting up X Y Grid expanding the values just past ...
    the dimensions of the
%dishes
xp = linspace(0,F(countF,count)+1,2000);
yp = linspace(0,D/2+.5,2000);
[Xp,Yp] = meshgrid(xp,yp);
% Min X and Y values for plot calcs
ymax=D/2;                % Limits this to the radius ...
    of the main reflector
ymin=0;                  % Only plan to plot
% Defined from the Parameterization of a parabolic curve
xmin=ymin.^2/(4*F(countF,count));
xmax=ymax.^2/(4*F(countF,count));
SRymin=0;                % SR limitations
SRymax=Ds/2;
% Sub reflector y limiting values
SRry=yp≥SRymin & yp≤SRymax;
SRry=yp(SRry);
% Hyp Calculations
Fp(countF,count)=F(countF,count);      % Focal length ...
    for the Main reflector
c(countF,count)=Fp(countF,count)/2;   % c-Hyperbolic ...
    curve parameter
```

```
e=1.2712;                               % e-eccentricity
a(countF,count)=c(countF,count)/e;     % a-Hyperbolic ...
    curve parameter.
% b-Hyperbolic curve parameter
b(countF,count)=sqrt(c(countF,count)^2...
-a(countF,count)^2)
% Recording Hyperbolic SR face location for later use
Lv(countF,count)=c(countF,count)+a(countF,count);
% X values for a hyperbolic SR
SRrxH=a(countF,count)*(sqrt(1+(SRry...
/b(countF,count)).^2)-1)+...
(c(countF,count)+a(countF,count)); % X values for a ...
    hyperbolic SR
m=max(SRrxH);   % Storing the max of X of the SR ...
    value for later use.
% Checking Angle from the source to edge of the SR
SRA(countF,count)=atand(SRymax/m);
TA=-10;                             % Edge Taper Value
psi=SRA(countF,count)*pi/180;      % Converting SRA ...
    to radians
% Calculating the value of N based on the input ...
    parameters.
N(countF,count)=log(10^(TA/10))/log(cos(psi/2))/2;
end
end
```

1.2 .oaa multifile tool

This script is used to load all data files of .oaa file type, and then produce plots and data analysis on the files loaded.

```
clc
clear all
close all
% Presetting generic variables
data=[];
%defining file type to automatically load data from
fileList = dir('*.oaa');
numFiles = length(fileList);
%looping among all files
for iter = 1:numFiles
% defining data and file name from oaa file
filename = fileList(iter).name;
data = dlmread(filename,',',1,0);
% Defining range of theta without repeating for phi
X=unique(data(:,1));
% Finding how many data points we have per Theta
ThetaLength = length(X);
% setting loop variable for how many times theta ...
    repeated
Repeat=max(histc(data(:,1),X));
% counting variables
```

```
SC=1;
PC=1; % Phi counter
Count=1;
clear YD % Saving space
for phi = 1:Repeat
% data start and end variables
DE=PC*ThetaLength;
DB=DE-ThetaLength+1;
% reference variables for start and end of data
g2(Count)=DE;
g1(Count)=DB;
P=(phi-1)*10;
% Magnitude Data for RHCP
YD(:,PC) = data(DB:DE,2);

%                   figure
%                   plot(X,YD(:,PC))
%                   ...
   FigName=sprintf('SixMNoStrutPhi%02d.fig',P);
%                   saveas(gcf,FigName,'fig');

PC=PC+1;
end
% Finds peaks of the side lobes saves reference ...
   location and values
[pks,locs] = ...
```

```
   findpeaks(YD(10:end,1),'MinPeakHeight',-20);
locs=X(locs);
% Main Lobe Peak and 3dB beamwidth
Max(iter)=max(YD(:,1));
HP(iter) = Max(iter)-3;
HPBW(iter)=2*(X(abs(HP(iter) - YD(:,1)) == ...
   min(abs(HP(iter) - YD(:,1)))));
% Breaks Peak data into specific side lobes
FSL(iter)=pks(1);
FSA(iter)=locs(1);
SSL(iter)=pks(2);
SSA(iter)=locs(2);
TSL(iter)=pks(3);
TSA(iter)=locs(3);
%Pull Data from Filename Change X:Y to follow naming ...
   scheme
%Section used to quickly label the parameter sweep ...
   values
range=3:5;
scale=100;
FN(iter,:)=str2num(filename(range))/scale;
%Plots each individual files Phi0 magnitude vs Theta
%     figure
%     hold on
%     plot(X,(YD(:,1)))
%     plot(locs,pks,'ro')
```

```
% %      FN2=sprintf('SiMTaper%02d.fig',iter-1)
% %      saveas(gcf,FN2,'fig')
end
%Normalizing magnitude points by the assumed value
MaxB=Max(end);
MaxN=Max(1:end-1)-MaxB;
HPBWB=HPBW(end);
HPBWN=HPBW(1:end-1);
FSLB=FSL(end);
FSLN=FSL(1:end-1)-FSLB;
FSAN=FSA(1:end-1);
SSLB=SSL(end);
SSLN=SSL(1:end-1)-SSLB;
SSAN=SSA(1:end-1);
TSLB=TSL(end);
TSLN=TSL(1:end-1)-TSLB;
TSAN=TSA(1:end-1);
FN=FN(1:end-1);
[MM MI]=max(MaxN(2:end));
%Setting up for plots and saving figures
filename='ESweep';
config='\fontsize{8}Config: Phi=0, Dm=6m, Ds/Dm=0.1, ...
    Taper=-10dB, F/Dm=0.3125';
xlab='Eccentricity';
figure
plot(FN,MaxN)
```

```
title({'\fontsize{14}Main Lobe Power';config})
xlabel(xlab)
ylabel('Magnitude in dB')
ylim([-5 5])
fileName = [filename 'max.png'];
saveas(gcf,fileName);
figure
plot(FN,HPBWN)
title({'\fontsize{14}Half Power Beamwidth';config})
xlabel(xlab)
ylabel('Beamwidth in degrees')
ylim([0.3 1.2])
fileName = [filename 'BW.png'];
saveas(gcf,fileName);
figure
[hAx,hLine1,hLine2] = plotyy(FN,FSLN,FN,FSAN);
title({'\fontsize{14}First Side Lobe';config})
xlabel(xlab)
ylabel(hAx(1),'Magnitude in dB') % left y-axis
ylabel(hAx(2),'Angle in degrees') % right y-axis
set(hAx(1),'Ylim',[-10 10])
set(hAx(1),'YTick',-10:1:10)
set(hAx(2),'Ylim',[0 5])
set(hAx(2),'YTick',0:.5:5)
fileName = [filename 'FSL.png'];
saveas(gcf,fileName);
```

```
figure
[hAx,hLine1,hLine2] = plotyy(FN,SSLN,FN,SSAN);
title({'\fontsize{14}Second Side Lobe';config})
xlabel(xlab)
ylabel(hAx(1),'Magnitude in dB') % left y-axis
ylabel(hAx(2),'Angle in degrees') % right y-axis
set(hAx(1),'Ylim',[-10 10])
set(hAx(1),'YTick',-10:1:10)
set(hAx(2),'Ylim',[0 5])
set(hAx(2),'YTick',0:.5:5)
fileName = [filename 'SSL.png'];
saveas(gcf,fileName);
figure
[hAx,hLine1,hLine2] = plotyy(FN,TSLN,FN,TSAN);
title({'\fontsize{14}Third Side Lobe';config})
xlabel(xlab)
ylabel(hAx(1),'Magnitude in dB') % left y-axis
ylabel(hAx(2),'Angle in degrees') % right y-axis
set(hAx(1),'Ylim',[-10 10])
set(hAx(1),'YTick',-10:1:10)
set(hAx(2),'Ylim',[0 5])
set(hAx(2),'YTick',0:.5:5)
fileName = [filename 'TSL.png'];
saveas(gcf,fileName);
```

Appendix B. Batch File Setup

Most of the simulations ran in this work were completed in SATCOM. In an effort to reduce the total simulation time, batch files were written to automate the process of starting new simulations. SATCOM generates a .ref file for the dual reflector analysis. Opening this .ref file with Satbench allows the file to be edited and revised as well as a host of other options associated with Satbench. Opening this software with OSUSACC Reflector Analysis automatically starts the simulation. Since the simulation can be started automatically by changing the program which opens it, this can be automated using batch files. Batch files at a basic level are DOS scripts which allow the automation of repetitive tasks. In this work all of the batch files started as text files and then saved as a .bat. Splitting all of the simulations which needed to be ran in to groups of batch files allowed for a significant amount of automation. Without using this sort of automation a person would have to select and start a new sim every time one finished. Setting up the simulations to run automatically from the batch files allowed for successive instant starts on new sims. At one time during this research project, 10 groups of simulations were run on 2 machines at one time. Batching the sims in this way saved a significant amount of calendar time to get the desired results. The following lines of script are a condensed edited version of the batch files used in this research.

```
start /wait /d ”File Location” SimName1.ref
start /wait /d ”File Location” SimName2.ref
start /wait /d ”File Location” SimNameBeforeLast.ref
start /wait /d ”File Location” SimNameLast.ref
```

Each line of this simple script follows the same flow. Each line essentially tells the computer to open SimNamX.ref which is located in ”File Location”, and then wait for SimNameX.ref to close prior to executing the next line.

Bibliography

[1] Peter J Collins. The 2-D Compact Range UTD Problem Approach Direct Ray. 2016.

[2] Peter W. Hannan. Microwave Antennas Derived from the Cassegrain Telescope. *IRE Transactions on Antennas and Propogation*, 1960.

[3] M. R. Ahsan, M. T. Islam, Y. Yamada, and N. Misran. Designing shaped dual reflector antenna system by ray tracing method. *International Conference on Space Science and Communication, IconSpace*, (July):285–289, 2013.

[4] Teh-Hong Lee, Roger C. Rudduck, and Kevin M. Lambert. Pattern Measurements of Reflector Antennas in the Compact Range and Validation with Computer Code Simulation. *IEEE Transactions on Antennas and Propagation*, 38(6), 1990.

[5] Hou Qin Qiu Shi, Liu Guozhi, Jiao Yongchang, Huang Wenhua. Three Reflector Beam Waveguide Application in High Power Microwave Antenna. *High Power and Particle Beams*, 22(1), 2010.

[6] Tie Zhu Liang, Wen Hua Huang, Hao Shao, Kang Yi Wang, Jia Wei Li, and Hui Jun Huang. Design and near field characteristic of high power microwave dual-reflector antenna. *2012 International Conference on Microwave and Millimeter Wave Technology, ICMMT 2012 - Proceedings*, 5:1746–1749, 2012.

[7] Tom Milligan and Christophe Granet. A simple procedure for the design of classical displaced-axis dual-reflector antennas using a set of geometric parameters. *IEEE Antennas and Propagation Magazine*, 41(6):64–71, 1999.

[8] G.T. Poulton. The Design of Cassegrain Antennas for High Efficiency and Low V.S.W.R. pages 61–65.

[9] A. Imani, M. Soleimani, and S. Amiri. Analysis of dual-reflector antenna for radar applications. *Applied Computational Electromagnetics Society Journal*, 30(12):1294–1300, 2015.

[10] Roger Ludwig Taylor and Jim. DESCANSO Design and Performance Summary Series Mars Global Surveyor. *Jpl*, 2002.

[11] Divya Gupta. A Review On Designing Of The Dual Reflector Axially Symmetric Cassegrain Antenna. *IOSR Journal of Electronics and Communication Engineering*, 4(1):48–51, 2012.

[12] Paul Wade. Multiple Reflector Dish Antennas. *Focus*, 2004.

[13] Josua M. Wilson. *The Design and Analysis of Electrically Large Custom-Shaped Reflector Antennas*. PhD thesis, Air Force Institute of Technology, 2013.

[14] D.A McNamara, C.W.I. Pistorius, and J.A.G. Malherbe. *Introduction to the uniform geometrical theory of diffraction*. 1990.

[15] Joseph B. Keller. Geometrical Theory of Diffraction*. *Journal of the Optical Society of America*, 52(2):116, feb 1962.

[16] Yahya Rahmat-Samii. GTD, UTD, UAT, and STD: A historical revisit and personal observations. *IEEE Antennas and Propagation Magazine*, 55(3):29–40, 2013.

[17] Enrique Nova, Daniel Rodrigo, Jordi Romeu, and Lluis Jofre. 94 GHz cassegrain reflector antenna performance characterization. *Proceedings of 6th European*

Conference on Antennas and Propagation, EuCAP 2012, (March):3442–3445, 2012.

[18] M. Thorbum. Large Antennas of the Deep Space Network [Book Review]. *IEEE Antennas and Propagation Magazine*, 46(1):110–111, 2004.

[19] Constatine A. Balanis. *Antenna Theory Analysis and Design.* John Wiley & Sons, Inc., third edition.

[20] A.J. Fenn and S. Srikanth. Green Bank Telescope 290 to 395 MHz Feed Analysis and Modification for Operation in the 140 to 175 MHz Band. Technical report, 2003.

[21] Christopher C. DeBoy, Christopher B. Haskins, Thomas A. Brown, Ronald C. Schulze, Mark A. Bernacik, J. Robert Jensen, Wesley Millard, Dennis Duven, and Stuart Hill. The RF telecommunications system for the new horizons mission to pluto. *IEEE Aerospace Conference Proceedings*, 3:1463–1476, 2004.

[22] Teh Hong Lee and Walter D. Burnside. Analysis of scattering from tapered and non-circular cross section struts for reflector antennas. *IEEE Antennas and Propagation Society, AP-S International Symposium (Digest)*, 4:128–131, 2002.

Acronyms

CEM computational electromagnetics. 2

GO geometric optics. 13

OSU Ohio State University. 29, 46, 86

PEC perfect electrical conductor. 3

PO physical optics. 4, 6, 7, 8, 10, 12, 16, 57, 58, 65, 66, 86

UTD uniform theory of diffraction. 4, 10, 12, 16, 30, 58, 86

REPORT DOCUMENTATION PAGE

Form Approved
OMB No. 0704–0188

1. REPORT DATE *(DD–MM–YYYY)*
27–03–2020

2. REPORT TYPE
Master's Thesis

3. DATES COVERED *(From — To)*
Sept 2018 — Mar 2020

4. TITLE AND SUBTITLE

Characterization and Sensitivity Analysis of
6 Meter Cassegrain Antenna

5a. CONTRACT NUMBER

5b. GRANT NUMBER

5c. PROGRAM ELEMENT NUMBER

6. AUTHOR(S)

Capt James L. Harris

5d. PROJECT NUMBER

5e. TASK NUMBER

5f. WORK UNIT NUMBER

7. PERFORMING ORGANIZATION NAME(S) AND ADDRESS(ES)

Air Force Institute of Technology
Graduate School of Engineering and Management (AFIT/EN)
2950 Hobson Way
WPAFB OH 45433-7765

8. PERFORMING ORGANIZATION REPORT NUMBER

AFIT-ENG-MS-20-M-025

9. SPONSORING / MONITORING AGENCY NAME(S) AND ADDRESS(ES)

Intentionally Left Blank

10. SPONSOR/MONITOR'S ACRONYM(S)

11. SPONSOR/MONITOR'S REPORT NUMBER(S)

12. DISTRIBUTION / AVAILABILITY STATEMENT

DISTRIBUTION STATEMENT A:
APPROVED FOR PUBLIC RELEASE; DISTRIBUTION UNLIMITED.

13. SUPPLEMENTARY NOTES

14. ABSTRACT

This paper will characterize a 6 meter in diameter Cassegrain antenna. Cassegrain antennas are a special form of a dual reflector antenna which uses a main reflector following a parabolic curve and a sub reflector which follows a hyperbolic curve. Cassegrain style antennas have multiple parameters which can be tuned to achieve specific design goals. Performing a sensitivity analysis will establish relationships between design parameters, directivity, side lobe levels, and effects of strut geometry. The initial design parameters will be assumed based on typical values. Results from the sensitivity analysis will be used to provide a performance band for the 6m Cassegrain at select frequencies.

15. SUBJECT TERMS

Dual Reflector Antennas, Cassegrain Antenna Design, Sensitivity Analysis

16. SECURITY CLASSIFICATION OF:			**17. LIMITATION OF ABSTRACT**	**18. NUMBER OF PAGES**	**19a. NAME OF RESPONSIBLE PERSON**
a. REPORT	**b. ABSTRACT**	**c. THIS PAGE**			Dr. Andrew J. Terzuoli, AFIT/ENG
					19b. TELEPHONE NUMBER *(include area code)*
U	U	U	UU	120	(937) 255-3636x4717; Andrew.Terzuoli@afit.edu